INTERNATIONAL JOURNAL OF
NUMERICAL ANALYSIS AND MODELING
Volume 17, Number 4, Pages 485–516

MULTILEVEL FINITE VOLUME METHODS FOR 2D INCOMPRESSIBLE NAVIER-STOKES EQUATIONS

J. K. DJOKO, H. H. GIDEY*, AND B. D. REDDY

Abstract. In this work, implicit and explicit multilevel finite volume methods have been constructed to solve the 2D Navier-Stokes equation with specified initial condition and boundary conditions. The multilevel methods are applied to the pressure-correction projection method using space finite volume discretization. The convective term is approximated by a linear expression that preserves the physical property of the continuous model. The stability analysis of the numerical methods have been discussed thoroughly by making use of the energy method. Numerical experiments exhibited to illustrate some differences between the new (multilevel) and conventional (one-level) schemes.

Key words. Navier-Stokes equations, stability, multilevel finite volume method.

1. Introduction

Let $\Omega = (0, L_1) \times (0, L_2) \subseteq \mathbb{R}^2$ be an open and bounded region in $\mathbb{R}^2$ with smooth boundary $\partial\Omega$ and points denoted by $(x, y) \in \overline{\Omega} = \Omega \cup \partial\Omega$. Let $\langle \cdot, \cdot \rangle$ denote the $L^2(\Omega)$ inner product of vectors or matrix fields on Ω, depending on the context; i.e.,

$$\langle \mathbf{u}, \mathbf{u} \rangle = \int_\Omega \mathbf{u} \cdot \mathbf{v} \, d\Omega, \tag{1}$$

where $\mathbf{u}$ and $\mathbf{v}$ are arbitrary vectors on Ω. The associated L^2-norm is denoted by $\| \cdot \| = \sqrt{\langle \cdot, \cdot \rangle}$. The spatial velocity field of the fluid filling the region $\overline{\Omega}$ is denoted by $\mathbf{u}(x, y, t)$, where $t \in [0, T]$, $T \in \mathbb{R}_+$.

The Navier-Stokes equations governing the dynamics of the viscous incompressible and homogeneous fluids is written in the generic form [1]

$$\mathbf{u}_t + B(\mathbf{u})\mathbf{u} = -\nabla p + \nu \Delta \mathbf{u} + f, \qquad \text{in } \Omega \tag{2}$$

$$\operatorname{div} \mathbf{u} = 0, \tag{3}$$

associated with the following boundary conditions and initial data:

$$\mathbf{u} = 0, \text{ on } \partial\Omega \tag{4}$$

$$\mathbf{u}|_{t=0} = \mathbf{u}_0 \quad \text{in} \quad \Omega, \tag{5}$$

where $B(\mathbf{u})\mathbf{u}$ is the convective term, $\nu > 0$ is the kinematic shear viscosity, p is a pressure field arising from incompressibility constraint div $\mathbf{u} = 0$ and f is applied body force.

Received by the editors July 29, 2019 and, in revised form, April 21, 2020.
2000 *Mathematics Subject Classification.* 65M12, 65M55, 65N12, 65N12, 65N55, 74S10.
*Corresponding author.

Let $\mathcal{H}$ be the space of $L^2(\Omega)$-smooth vector fields tangent to the boundary $\partial\Omega$ and denote by $\mathcal{H}_{\text{div}}$ the subspace of divergence-free vector fields:

$$\mathcal{H} := \{\mathbf{u} \in L^2(\Omega)^2 : \mathbf{u}(0,y,t) = \mathbf{u}(L_1,y,t) = \mathbf{u}(x,0,t) = \mathbf{u}(x,L_2,t) = 0, \tag{6}$$

$$x \in [0,L_1], y \in [0,L_2]\} \tag{7}$$

$$\mathcal{H}_{\text{div}} := \{\mathbf{u} \in \mathcal{H} : \text{ div } \mathbf{u} = 0\}. \tag{8}$$

In this study, we consider the standard form of the convective term, i.e, $B(\mathbf{u})\boldsymbol{\eta} = (\mathbf{u}\cdot\nabla)\boldsymbol{\eta}$, for any smooth $H^1(\Omega)$-vector field $\boldsymbol{\eta}$, with associated pressure field denoted by p. Using integration by parts, we obtain

$$\langle B(\mathbf{u})\boldsymbol{\eta}_1, \boldsymbol{\eta}_2\rangle = -\langle \boldsymbol{\eta}_1, B(\mathbf{u})\boldsymbol{\eta}_2\rangle - \langle \text{div}\mathbf{u}\,\boldsymbol{\eta}_1, \boldsymbol{\eta}_2\rangle + \int_\Gamma (\mathbf{u}\boldsymbol{\eta}_1 \cdot \boldsymbol{\eta}_2)(\mathbf{u}\cdot\mathbf{n})d\Gamma, \tag{9}$$

for arbitrary $H^1(\Omega)$-smooth vector fields $\boldsymbol{\eta}_1, \boldsymbol{\eta}_2$ on Ω.

$$\langle B(\mathbf{u})\boldsymbol{\eta}_1, \boldsymbol{\eta}_2\rangle = -\langle \boldsymbol{\eta}_1, B(\mathbf{u})\boldsymbol{\eta}_2\rangle, \mathbf{u} \in \mathcal{H}_{\text{div}}. \tag{10}$$

$$\langle B(\mathbf{u})\boldsymbol{\eta}, \boldsymbol{\eta}\rangle = 0, \text{ for any } H^1(\Omega) \text{ smooth vector field } \boldsymbol{\eta}, \tag{11}$$

only holds if the velocity field is divergence-free; $\mathbf{u} \in \mathcal{H}_{\text{div}}$.

Integrating equation (3) over a control volume and converting the volume integral to a surface integral gives

$$\int_\Omega \text{div } \mathbf{u}\, dx\, dy = \oint_S \mathbf{u}\cdot\mathbf{n}\, dx\, dy = 0. \tag{12}$$

This shows that the inflow must be equal to the outflow.

Our objective is to construct multilevel finite volume methods based on the work in [2-4] to compute the numerical solution of (2)-(5). Multilevel methods were introduced to improve calculation speed in the simulation of complex physical phenomena while maintaining good accuracy [3-8]. We construct implicit and explicit finite volume methods based on the work of Appadu et al. [2] and Bousquet et al. [4]. The schemes we construct are easy to implement and the convective term $B(\mathbf{u})\mathbf{u}$ is approximated such that the discrete analogue of the property (11) holds.

Our work can also be seen as continuation of investigations started in [1] because in a way we are concerned with the stability of the new schemes that should preserve (11). The main difference with the former investigation is that we are dealing here with multilevel scheme, hence stability analysis is more complex, even with the use of a simpler technique (energy method). We do not discuss existence of solutions of the schemes formulated because we are dealing with linear scheme (for the implicit multilevel method) and explicit multilevel method. Hence solvability of the implicit scheme is a consequence of Lax-Milgram's result in the discrete setting.

The next section is devoted to space discretization and some properties that are helpful to our study. In section 3, we are concerned with the multilevel discretization and time stepping algorithm. In sections 4 and 5, we present the implicit and explicit multilevel finite volume methods, respectively and analyse their stability. In section 6, we present the numerical results obtained from the two multilevel methods and these results are compared with the full one-level finite volume methods on the fine mesh and coarse mesh. Concluding remarks and some open questions are reported in section 7.

2. Some properties and space discretizations

In this section, we present the space discretization in a 2D rectangular region. To develop finite volume approximations that satisfy the discrete analogue of (11), we first introduce some standard notations and results. Let Δx and Δy are the spatial step sizes in the $x-$ and $y-$ directions, respectively and let $(k_{i,j})$ is the (i,j) control volume of uniform area $\Delta x \Delta y$. Let N_1 and N_2 are integers such that $\Delta x\, N_1 = L_1$ and $\Delta y\, N_2 = L_2$. For $0 \le i \le N_1$ and $0 \le j \le N_2$,

$$x_{i+1/2} = i\Delta x,\ y_{j+1/2} = j\Delta y,$$

so that

$$k_{i,j} = (x_{i-1/2}, x_{i+1/2}) \times (y_{j-1/2}, y_{j+1/2}), \quad 1 \le i \le N_1, 1 \le j \le N_2.$$

(x_i, y_j) is the centre of the (i,j) control volume, which is given by the formula

$$(x_i, y_j) = \left((i-1)\Delta x + \frac{\Delta x}{2},\ (j-1)\Delta y + \frac{\Delta y}{2}\right).$$

In the rest of this work, we take $h = (\Delta x, \Delta y)$. The approximate solutions, the velocities and pressure, to the control volume average of the true solution at $t_n = n\Delta t$ are given by

$$\mathbf{u}^n_{i,j} \approx \frac{1}{\Delta x \Delta y} \iint\limits_{k_{i,j}} \mathbf{u}(x,y,t_n)dxdy \qquad \text{for the velocity},$$

$$p^n_{i,j} \approx \frac{1}{\Delta x \Delta y} \iint\limits_{k_{i,j}} p(x,y,t_n)dxdy \qquad \text{for the pressure},$$

for $i = 1, 2, \ldots, N_1$ and $j = 1, 2, \ldots, N_2$ where Δt is the temporal step size such that $\Delta t M = T$, which is obtained recursively by starting with the initial average value, $\mathbf{u}^0_{i,j}$, given by

$$\mathbf{u}^0_{i,j} = \frac{1}{\Delta x \Delta y} \iint\limits_{k_{i,j}} \mathbf{u}^0(x,y)dxdy.$$

To take into account the boundary conditions we introduce the fictitious cells (ghost-cells)

$$\begin{aligned} k_{0,j} &= (-\Delta x, 0) \times ((j-1)\Delta y, j\Delta y), j = 1, \ldots, N_2, \\ k_{N_1+1,j} &= (L_1, L_1 + \Delta x) \times ((j-1)\Delta y, j\Delta y), j = 1, \ldots, N_2, \\ k_{i,0} &= ((i-1)\Delta x, i\Delta x) \times (-\Delta y, 0), i = 1, \ldots, N_1, \\ k_{i,N_2+1} &= ((i-1)\Delta x, i\Delta x) \times (L_2, L_2 + \Delta y), i = 1, \ldots, N_1. \end{aligned}$$

Define the spaces $\mathcal{H}_h$ and $\mathcal{H}_h^{\mathrm{div}}$ as

$$\mathcal{H}_h = \left\{ \mathbf{u} = \left(\mathbf{u}_{i,j}\right)_{i,j}, \mathbf{u}_{i,j} \in \mathbb{R}^2 \middle|\ \mathbf{u}_{0,j} = \mathbf{u}_{i,0} = \mathbf{u}_{N_1+1,j} = \mathbf{u}_{i,N_2+1} = 0 \right\},$$

and

$$\mathcal{H}_h^{\mathrm{div}} = \left\{ \mathbf{u} \in \mathcal{H}_h \middle|\ \mathrm{div}\ \mathbf{u} = 0 \right\},$$

equipped with the inner product and discrete L^2 norm

$$(\mathbf{u},\mathbf{v})_h = \Delta x\Delta y\sum_{i=1}^{N_1}\sum_{j=1}^{N_2}\mathbf{u}_{i,j}\cdot\mathbf{v}_{i,j} \quad\text{and}\quad \|\mathbf{u}\|_h = \left(\Delta x\Delta y\sum_{i=1}^{N_1}\sum_{j=1}^{N_2}|\mathbf{u}_{i,j}|^2\right)^{1/2},$$

respectively, $h=(\Delta x,\Delta y)$.

For $\mathbf{u}\in\mathcal{H}_h$, we introduce the following difference operators:

$$\nabla^-_{1,h}\mathbf{u}_{i,j} = \frac{1}{\Delta x}\left(\mathbf{u}_{i,j}-\mathbf{u}_{i-1,j}\right),\ \nabla^+_{1,h}\mathbf{u}_{i,j} = \frac{1}{\Delta x}\left(\mathbf{u}_{i+1,j}-\mathbf{u}_{i,j}\right), \tag{13}$$

$$\nabla^-_{2,h}\mathbf{u}_{i,j} = \frac{1}{\Delta y}\left(\mathbf{u}_{i,j}-\mathbf{u}_{i,j-1}\right),\ \nabla^+_{2,h}\mathbf{u}_{i,j} = \frac{1}{\Delta y}\left(\mathbf{u}_{i,j+1}-\mathbf{u}_{i,j}\right), \tag{14}$$

$$\Delta_{1,h}\mathbf{u}_{i,j} = \frac{1}{\Delta x^2}\left(\mathbf{u}_{i+1,j}-2\mathbf{u}_{i,j}+\mathbf{u}_{i-1,j}\right), \tag{15}$$

$$\Delta_{2,h}\mathbf{u}_{i,j} = \frac{1}{\Delta y^2}\left(\mathbf{u}_{i,j+1}-2\mathbf{u}_{i,j}+\mathbf{u}_{i,j-1}\right), \tag{16}$$

From (13)-(16), we have

(17)

$$\nabla^\pm_h\mathbf{u}_{i,j} = \begin{pmatrix}\nabla^\pm_{1,h}u_{i,j} & \nabla^\pm_{2,h}u_{i,j}\\ \nabla^\pm_{1,h}v_{i,j} & \nabla^\pm_{2,h}v_{i,j}\end{pmatrix},\ \nabla^\pm_h u_{i,j} = \begin{pmatrix}\nabla^\pm_{1,h}u_{i,j}\\ \nabla^\pm_{2,h}u_{i,j}\end{pmatrix},\ \Delta_h = \Delta_{1,h}+\Delta_{2,h}.$$

The discrete analogue of the derivative of product of functions is given as follows: for $\mathbf{u},\mathbf{v}\in\mathcal{H}_h$,

$$\nabla^+_{1,h}(u_{i,j}v_{i,j}) = (\nabla^+_{1,h}u_{i,j})v_{i+1,j} + u_{i,j}(\nabla^+_{1,h}v_{i,j}), \tag{18}$$

$$\nabla^+_{2,h}(u_{i,j}v_{i,j}) = (\nabla^+_{2,h}u_{i,j})v_{i,j+1} + u_{i,j}(\nabla^+_{2,h}v_{i,j}), \tag{19}$$

$$\nabla^-_{1,h}(u_{i,j}v_{i,j}) = (\nabla^-_{1,h}u_{i,j})v_{i-1,j} + u_{i,j}(\nabla^-_{1,h}v_{i,j}), \tag{20}$$

$$\nabla^-_{2,h}(u_{i,j}v_{i,j}) = (\nabla^-_{2,h}u_{i,j})v_{i,j-1} + u_{i,j}(\nabla^-_{2,h}v_{i,j}). \tag{21}$$

We define the following semi-norm and norm

$$|\mathbf{u}|_{1,h} = \left(\Delta x\Delta y\sum_{i=1}^{N_1+1}\sum_{j=1}^{N_2+1}(\nabla^-_{1,h}u_{i,j})^2+(\nabla^-_{2,h}u_{i,j})^2+(\nabla^-_{1,h}v_{i,j})^2+(\nabla^-_{2,h}v_{i,j})^2\right)^{\frac{1}{2}},$$

$$\|\mathbf{u}\|_{h,\infty} = \max\{\max_{i,j}|u_{i,j}|,\max_{i,j}|v_{i,j}|\}$$

where $\mathbf{u} = \begin{pmatrix}\boldsymbol{u}\\ \boldsymbol{v}\end{pmatrix}$. We also have the following relations from the semi-discrete norms:

$$|\mathbf{u}|^2_{1,h} \le \left(\frac{4}{\Delta x^2}+\frac{4}{\Delta y^2}\right)\|\mathbf{u}\|^2_h, \tag{22}$$

$$\|\mathbf{u}\|^2_{h,\infty} \le \frac{1}{\Delta x\,\Delta y}\|\mathbf{u}\|^2_h. \tag{23}$$

From the definition of $\mathcal{H}_h$ and the discrete product rules (18) - (21), one obtains

Lemma 2.1. *Let $\boldsymbol{u},\boldsymbol{w}\in\mathcal{H}_h$. Then for $k=1,2$*

$$\sum_{i=1}^{N_1}\sum_{j=1}^{N_2}\boldsymbol{w}_{i,j}\cdot(\nabla^+_{k,h}\boldsymbol{u}_{i,j}) = -\sum_{i=1}^{N_1}\sum_{j=1}^{N_2}\boldsymbol{u}_{i,j}\cdot(\nabla^-_{k,h}\boldsymbol{w}_{i,j}).$$

For any $\mathbf{u}, \mathbf{w} \in \mathcal{H}_h$

$$2(\mathbf{u}-\mathbf{w}, \mathbf{u})_h = \|\mathbf{u}\|_h^2 - \|\mathbf{w}\|_h^2 + \|\mathbf{u}-\mathbf{w}\|_h^2, \tag{24}$$

$$2(\mathbf{u}-\mathbf{w}, \mathbf{w})_h = \|\mathbf{u}\|_h^2 - \|\mathbf{w}\|_h^2 - \|\mathbf{u}-\mathbf{w}\|_h^2. \tag{25}$$

It is important to note that if $\mathbf{u}$ belongs to $\mathcal{H}_h$, then the discrete Poincaré's inequality holds; this is to say that there is $c_0 > 0$, independent of Δx and Δy such that

$$\|\mathbf{u}\|_h \le c_0 |\mathbf{u}|_{1,h}. \tag{26}$$

For $x \in [0, 1/2]$ we have

$$1 - x \ge 2^{-2x}. \tag{27}$$

In order to approximate the nonlinear term such that the discrete analogue of (11) holds, we introduce the bilinear map: $C_h : \mathcal{H}_h \times \mathcal{H}_h \to (\mathbb{R}^2)^{N_1\times N_2}$ in the form

$$C_h(\mathbf{u}, \mathbf{w})_{i,j} = \begin{pmatrix} C_h^u(\mathbf{u}, \mathbf{w})_{i,j} \\ C_h^v(\mathbf{u}, \mathbf{w})_{i,j} \end{pmatrix}, \tag{28}$$

where

$$\begin{aligned} C_h^u(\mathbf{u}, \mathbf{w})_{i,j} = \alpha_1 \Big[& w_{i,j}\nabla_{1,h}^+ u_{i,j} + u_{i,j}\nabla_{1,h}^- w_{i,j} \\ & + u_{i+1,j}\nabla_{1,h}^+ w_{i,j} + w_{i,j}\nabla_{2,h}^+ v_{i,j} + v_{i,j}\nabla_{2,h}^- w_{i,j} + v_{i,j+1}\nabla_{2,h}^+ w_{i,j}\Big] \\ + \alpha_2 \Big[& w_{i,j}\nabla_{1,h}^- u_{i,j} + u_{i,j}\nabla_{1,h}^+ w_{i,j} + u_{i-1,j}\nabla_{1,h}^- w_{i,j} \\ & + w_{i,j}\nabla_{2,h}^- v_{i,j} + v_{i,j}\nabla_{2,h}^+ w_{i,j} + v_{i,j-1}\nabla_{2,h}^- w_{i,j}\Big], \end{aligned} \tag{29}$$

$$\begin{aligned} C_h^v(\mathbf{u}, \mathbf{w})_{i,j} = \alpha_1 \Big[& s_{i,j}\nabla_{1,h}^+ u_{i,j} + u_{i,j}\nabla_{1,h}^- s_{i,j} \\ & + u_{i+1,j}\nabla_{1,h}^+ s_{i,j} + s_{i,j}\nabla_{2,h}^+ v_{i,j} + v_{i,j}\nabla_{2,h}^- s_{i,j} + v_{i,j+1}\nabla_{2,h}^+ s_{i,j}\Big] \\ & + \alpha_2 \Big[s_{i,j}\nabla_{1,h}^- u_{i,j} + u_{i,j}\nabla_{1,h}^+ s_{i,j} + u_{i-1,j}\nabla_{1,h}^- s_{i,j} \\ & + s_{i,j}\nabla_{2,h}^- v_{i,j} + v_{i,j}\nabla_{2,h}^+ s_{i,j} + v_{i,j-1}\nabla_{2,h}^- s_{i,j}\Big], \end{aligned} \tag{30}$$

$$\mathbf{u} = \begin{pmatrix} \boldsymbol{u} \\ \boldsymbol{v} \end{pmatrix}, \qquad \mathbf{w} = \begin{pmatrix} \boldsymbol{w} \\ \boldsymbol{s} \end{pmatrix},$$

and α_1 and α_2 are constants.

Lemma 2.2. *For any $\boldsymbol{u}, \boldsymbol{w} \in \mathcal{H}_h$, the following hold.*

$$(C_h(\boldsymbol{u}, \boldsymbol{w}), \boldsymbol{w})_h = 0. \tag{31}$$

$$|(C_h(\boldsymbol{u}, \boldsymbol{u}), \boldsymbol{w})_h| \le 3\sqrt{2}\Big(|\alpha_1| + |\alpha_2|\Big)\|\boldsymbol{u}\|_{h,\infty}|\boldsymbol{u}|_{1,h}\|\boldsymbol{w}\|_h. \tag{32}$$

Proof. Let $\mathbf{u} = \begin{pmatrix} \boldsymbol{u} \\ \boldsymbol{v} \end{pmatrix}, \mathbf{w} = \begin{pmatrix} \boldsymbol{w} \\ \boldsymbol{s} \end{pmatrix}$. From the definition of the discrete inner product, we have

$$(C_h(\mathbf{u}, \mathbf{w}), \mathbf{w})_h = \Delta x \Delta y \sum_{i=1}^{N_1}\sum_{j=1}^{N_2} \left[C_h^u(\mathbf{u}, \mathbf{w})_{i,j} w_{i,j} + C_h^v(\mathbf{u}, \mathbf{w})_{i,j} s_{i,j}\right].$$

We see each of the terms in (29) and (30) and apply Lemma 2.1. From the definition of the discrete operators, we have

$$w_{i,j}\nabla_{1,h}^{+}u_{i,j}w_{i,j} = w_{i,j}\nabla_{1,h}^{+}(u_{i,j}w_{i,j}) - w_{i,j}(\nabla_{1,h}^{+}w_{i,j})u_{i+1,j},$$

and then taking the sum and applying Lemma (2.1), we obtain

$$\begin{aligned}\sum_{i=1}^{N_1}\sum_{j=1}^{N_2} w_{i,j}\nabla_{1,h}^{+}u_{i,j}w_{i,j} &= \sum_{i=1}^{N_1}\sum_{j=1}^{N_2} w_{i,j}\nabla_{1,h}^{+}(u_{i,j}w_{i,j}) - \sum_{i=1}^{N_1}\sum_{j=1}^{N_2} w_{i,j}(\nabla_{1,h}^{+}w_{i,j})u_{i+1,j},\\ &= -\sum_{i=1}^{N_1}\sum_{j=1}^{N_2} w_{i,j}\Big[u_{i,j}\nabla_{1,h}^{-}w_{i,j} + u_{i+1,j}\nabla_{1,h}^{+}w_{i,j}\Big].\end{aligned}$$

Similarly, we obtain

$$\begin{aligned}\sum_{i=1}^{N_1}\sum_{j=1}^{N_2} w_{i,j}\nabla_{1,h}^{-}u_{i,j}w_{i,j} &= -\sum_{i=1}^{N_1}\sum_{j=1}^{N_2} w_{i,j}\Big[u_{i,j}\nabla_{1,h}^{+}w_{i,j} + u_{i-1,j}\nabla_{1,h}^{-}w_{i,j}\Big],\\ \sum_{i=1}^{N_1}\sum_{j=1}^{N_2} w_{i,j}\nabla_{2,h}^{+}v_{i,j}w_{i,j} &= -\sum_{i=1}^{N_1}\sum_{j=1}^{N_2} w_{i,j}\Big[v_{i,j}\nabla_{2,h}^{-}w_{i,j} + v_{i,j+1}\nabla_{2,h}^{+}w_{i,j}\Big],\\ \sum_{i=1}^{N_1}\sum_{j=1}^{N_2} w_{i,j}\nabla_{2,h}^{-}v_{i,j}w_{i,j} &= -\sum_{i=1}^{N_1}\sum_{j=1}^{N_2} w_{i,j}\Big[v_{i,j}\nabla_{2,h}^{+}w_{i,j} + u_{i,j-1}\nabla_{2,h}^{-}w_{i,j}\Big].\end{aligned}$$

Thus using the definition of C_h^u, we obtain

$$\sum_{i=1}^{N_1}\sum_{j=1}^{N_2} C_h^u(\mathbf{u},\mathbf{w})_{i,j}w_{i,j} = 0. \tag{33}$$

In a similar way, we obtain

$$\sum_{i=1}^{N_1}\sum_{j=1}^{N_2} C_h^v(\mathbf{u},\mathbf{w})_{i,j}s_{i,j} = 0, \tag{34}$$

and hence the first argument of the Lemma, (31), holds.

To prove the inequality, we majorize each of the terms in the inner product. From the definition of C_h, we have

$$(C_h(\mathbf{u},\mathbf{u}),\mathbf{w})_h = \Delta x\Delta y\sum_{i=1}^{N_1}\sum_{j=1}^{N_2}\left[C_h^u(\mathbf{u},\mathbf{u})_{i,j}w_{i,j} + C_h^v(\mathbf{u},\mathbf{u})_{i,j}s_{i,j}\right].$$

$$
\begin{aligned}
&\Delta x\Delta y\sum_{i=1}^{N_1}\sum_{j=1}^{N_2} C_h^u(\mathbf{u},\mathbf{u})_{i,j}w_{i,j}\\
=&\Delta x\Delta y\sum_{i=1}^{N_1}\sum_{j=1}^{N_2}\Big[\alpha_1\Big(u_{i,j}\nabla^+_{1,h}u_{i,j}+u_{i,j}\nabla^-_{1,h}u_{i,j}+u_{i+1,j}\nabla^+_{1,h}u_{i,j}\Big)w_{i,j}\\
&+\alpha_1\Big(u_{i,j}\nabla^+_{2,h}v_{i,j}+v_{i,j}\nabla^-_{2,h}u_{i,j}+v_{i,j+1}\nabla^+_{2,h}u_{i,j}\Big)w_{i,j}\\
&+\alpha_2\Big(u_{i,j}\nabla^-_{1,h}u_{i,j}+u_{i,j}\nabla^+_{1,h}u_{i,j}+u_{i-1,j}\nabla^-_{1,h}u_{i,j}\Big)w_{i,j}\\
&+\alpha_2\Big(u_{i,j}\nabla^-_{2,h}v_{i,j}+v_{i,j}\nabla^+_{2,h}u_{i,j}+v_{i,j-1}\nabla^-_{2,h}u_{i,j}\Big)w_{i,j}\Big]\\
=&\alpha_1(I_1+I_2)+\alpha_2(I_3+I_4).
\end{aligned}
$$

To majorize the terms I_1, I_2, I_3 and I_4, we use the fact that

(35)
$$
\sum_{i=1}^{N_1}\sum_{j=1}^{N_2}u_{i,j}\nabla^+_{1,h}u_{i,j}w_{i,j}=\sum_{i=0}^{N_1}\sum_{j=1}^{N_2}u_{i,j}\nabla^+_{1,h}u_{i,j}w_{i,j}=\sum_{i=1}^{N_1+1}\sum_{j=1}^{N_2}u_{i-1,j}\nabla^-_{1,h}u_{i,j}w_{i-1,j}.
$$

Then

$$
\begin{aligned}
|I_1|\le&\Delta x\Delta y\sum_{i=1}^{N_1+1}\sum_{j=1}^{N_2}\Big(|u_{i-1,j}||\nabla^-_{1,h}u_{i,j}||w_{i-1,j}|\\
&+|u_{i,j}||\nabla^-_{1,h}u_{i,j}||w_{i,j}|+|u_{i,j}||\nabla^-_{1,h}u_{i,j}||w_{i-1,j}|\Big)\\
\le&\|\mathbf{u}\|_{h,\infty}\Delta x\Delta y\sum_{i=1}^{N_1+1}\sum_{j=1}^{N_2}\Big(|\nabla^-_{1,h}u_{i,j}||w_{i-1,j}|+|\nabla^-_{1,h}u_{i,j}||w_{i,j}|+|\nabla^-_{1,h}u_{i,j}||w_{i-1,j}|\Big)
\end{aligned}
$$

(36)
$$
\le 3\|\mathbf{u}\|_{h,\infty}\left(\Delta x\Delta y\sum_{i=1}^{N_1+1}\sum_{j=1}^{N_2}(\nabla^-_{1,h}u_{i,j})^2\right)^{1/2}\left(\Delta x\Delta y\sum_{i=1}^{N_1}\sum_{j=1}^{N_2}w_{i,j}^2\right)^{1/2}.
$$

In a similar way, we have

$$
\begin{aligned}
|I_2|,|I_4|\le&\|\mathbf{u}\|_{h,\infty}\left[\left(\Delta x\Delta y\sum_{i=1}^{N_1+1}\sum_{j=1}^{N_2}(\nabla^-_{2,h}v_{i,j})^2\right)^{1/2}\right.\\
&\left.+2\left(\Delta x\Delta y\sum_{i=1}^{N_1}\sum_{j=1}^{N_2+1}(\nabla^-_{2,h}u_{i,j})^2\right)^{1/2}\right]\times\left(\Delta x\Delta y\sum_{i=1}^{N_1}\sum_{j=1}^{N_2}w_{i,j}^2\right)^{1/2},
\end{aligned}
\tag{37}
$$

and

$$
|I_3|\le 3\|\mathbf{u}\|_{h,\infty}\left(\Delta x\Delta y\sum_{i=1}^{N_1+1}\sum_{j=1}^{N_2}(\nabla^-_{1,h}u_{i,j})^2\right)^{1/2}\left(\Delta x\Delta y\sum_{i=1}^{N_1}\sum_{j=1}^{N_2}w_{i,j}^2\right)^{1/2}.
\tag{38}
$$

Using (36)-(38), we obtain

(39)

$$|\Delta x\Delta y\sum_{i=1}^{N_1}\sum_{j=1}^{N_2}C_h^u(\mathbf{u},\mathbf{u})_{i,j}w_{i,j}|\leq 3(|\alpha_1|+|\alpha_2|)\|\mathbf{u}\|_{h,\infty}|\mathbf{u}|_{1,h}\left(\Delta x\Delta y\sum_{i=1}^{N_1}\sum_{j=1}^{N_2}w_{i,j}^2\right)^{\frac{1}{2}}.$$

Similarly, we obtain

(40)

$$|\Delta x\Delta y\sum_{i=1}^{N_1}\sum_{j=1}^{N_2}C_h^v(\mathbf{u},\mathbf{u})_{i,j}s_{i,j}|\leq 3(|\alpha_1|+|\alpha_2|)\|\mathbf{u}\|_{h,\infty}|\mathbf{u}|_{1,h}\left(\Delta x\Delta y\sum_{i=1}^{N_1}\sum_{j=1}^{N_2}s_{i,j}^2\right)^{\frac{1}{2}}.$$

Combining (39) and (40), we obtain (32). Hence the proof is complete. □

3. Multilevel discretization and time stepping algorithm

Multilevel methods were introduced to improve calculation speed in the simulation of complex physical phenomena while maintaining a good level of accuracy, see [3-8]. This section is an application of the work presented in [4], in which the shallow water equations are analyzed. Here, we are concerned with the two dimensional incompressible Navier-Stokes equations (2)-(3) with Dirichlet boundary conditions. We formulate in the spirit of [4] two methods approximating (2)-(3), namely: an implicit multilevel finite volume method and an explicit multilevel finite volume method. These new methods are next studied thoroughly and compared with respect to L^2-errors and CPU time with the associated one-level methods. To make this text self-contained for the reader, we recall below the multilevel finite volume approximation as described in Appadu et al. [2] and Bousquet et. al. [4].

Since the number of control volumes on the fine mesh is a multiple of three, we replace N_1 and N_2 in section 2 by $3N_1$ and $3N_2$, respectively such that $3N_1\Delta x = L_1$ and $3N_2\Delta y = L_2$. We discretize Ω into fine meshes and coarse meshes. The fine mesh consists of $3N_1 \times 3N_2$ regular cells $(k_{i,j})_{1\leq i\leq 3N_1, 1\leq j\leq 3N_2}$ of uniform area $\Delta x\Delta y$. The coarse mesh consists of N_1N_2 control volumes $(K_{l,m})_{1\leq l\leq N_1, 1\leq m\leq N_2}$ of uniform area $9\Delta x\Delta y$, where

$$K_{l,m} = (x_{3l-2-1/2}, x_{3m+1/2}) \times (y_{3m-2-1/2}, y_{3m+1/2}).$$

We denote the approximate solutions on the fine grid by $u_{i,j}$, $1 \leq i \leq 3N_1, 1 \leq j \leq 3N_2$. The approximation on the coarse mesh is given by

$$\mathbf{U}_{l,m} = \frac{1}{9}\sum_{\alpha,\beta=0}^{2}\mathbf{u}_{3l-\alpha,3m-\beta}, 1\leq l\leq N_1, 1\leq m\leq N_2,$$

and the incremental unknowns are given by the relation

$$\mathbf{Z}_{3l-\alpha,3m-\beta} = \mathbf{u}_{3l-\alpha,3m-\beta} - \mathbf{U}_{l,m}. \tag{41}$$

Let M be an integer such that $\Delta tM = T$. Let $\tau > 1$ and $q > 1$ be two fixed integers. We discretize (2) on the fine mesh by using time step $\Delta t/\tau$ and on the coarse mesh by using time step Δt. We assume that n is a multiple of $q+1$ and $(\mathbf{u}_{i,j}^n)_{1\leq i\leq 3N_1, 1\leq j\leq 3N_2}$ are known, where $\mathbf{u}_{i,j}^n$ is an approximation of the average value of $\mathbf{u}$ over $k_{i,j}$ at the grid $t = n\Delta t$, for $i = 1,\ldots,3N_1$, $j = 1,\ldots,3N_2$. For $r = 0,1,\ldots,\tau$ and $s = 1,2,\ldots,q+1$, we let $\mathbf{u}_{i,j}^{n+r/\tau}$ be the approximate solution of the mean values over $k_{i,j}$ at time $t_{n+t/\tau} = n\Delta t + r\Delta t/\tau$ for $i = 1,\ldots,3N_1, j =$

$1, \ldots, 3N_2$ and $\mathbf{U}_{l,m}^{n+s}$ the approximate solution of the mean value on the coarse mesh $K_{l,m}$ at time $t_{n+s} = (n+s)\Delta t$ for $l = 1, \ldots, N_1$ and $m = 1, \ldots, N_2$.

Remark 3.1. *Note that the ghost-cells are defined for both fine and coarse discretizations.*

At each time step, we use the fractional step/projection method to to solve the full problem (2)-(5) in a sequence of decoupled equations for the velocity and pressure. The concept of projection methods was introduced by Chorin et al. [9]; since then, several projection methods have been developed: see [10-13]. In this study, we consider for simplicity the pressure-correction projection method of Chorin et al. [9].

4. Implicit method

In this section based on the works of Chorin et al. [9] and Bousquet et al. [4], we construct a linearized implicit multilevel finite volume scheme. The nonlinear convective term $(\mathbf{u} \cdot \nabla)\mathbf{u}$ is approximated in a linear way using the bilinear map C_h defined by (28). The approximation of the convective term on the fine mesh is given as follows:

$$(\mathbf{u} \cdot \nabla)\mathbf{u}\Big|_{t=\Delta t(n+(r+1)/\tau)} \approx C_h(\tilde{\mathbf{u}}^{n+r/\tau}, \mathbf{u}^{n+(r+1)/\tau}),$$

where $\tilde{\mathbf{u}}^{n+r/\tau} = a_0\mathbf{u}^{n+r/\tau} + a_1\mathbf{u}^{n+(r-1)/\tau} + \cdots + a_{r_0}\mathbf{u}^{n+(r-r_0)/\tau}$, for $r > r_0$ with $a_0 + a_1 + \cdots + a_{r_0} = 1$, ensuring consistency. For $\lambda \le r_0$, $\tilde{\mathbf{u}}^{n+\lambda/\tau} = \mathbf{u}^{n+\lambda/\tau}$. The approximation of the convective term of the coarse mesh can be defined in a similar way.

For $r = 0, 1, \ldots, \tau - 1$ and $s = 1, 2, \ldots, q$, we discretize (2)-(3) as follows:

$$\begin{aligned} &\frac{\tau}{\Delta t}(\widehat{\mathbf{u}}_{i,j}^{n+(r+1)/\tau} - \mathbf{u}_{i,j}^{n+r/\tau}) + C_h(\tilde{\mathbf{u}}^{n+r/\tau}, \widehat{\mathbf{u}}^{n+(r+1)/\tau})_{i,j} \\ &= \nu\Delta_h\widehat{\mathbf{u}}_{i,j}^{n+(r+1)/\tau} + \mathbf{f}_{i,j}^{n+(r+1)/\tau}, \end{aligned} \tag{42}$$

$$\frac{\tau}{\Delta t}(\mathbf{u}_{i,j}^{n+(t+1)/\tau} - \widehat{\mathbf{u}}_{i,j}^{n+(r+1)/\tau}) = -\nabla_h^- p_{i,j}^{n+(r+1)/\tau}, \tag{43}$$

$$\nabla_h^+ \cdot \mathbf{u}_{i,j}^{n+(r+1)/\tau} = 0, \tag{44}$$

$$\mathbf{u}_{0,j}^{n+(r+1)/\tau} = \mathbf{u}_{3N_1+1,j}^{n+(r+1)/\tau} = \mathbf{u}_{i,3N_2+1}^{n+(r+1)/\tau} = \mathbf{u}_{i,0}^{n+(r+1)/\tau} = 0, \tag{45}$$

$$\mathbf{u}_{i,j}^0 = \frac{1}{\Delta x \Delta y}\iint_{k_{i,j}} \mathbf{u}_0(x,y)\,dx\,dy, \tag{46}$$

$$\frac{1}{\Delta t}(\widehat{\mathbf{U}}_{l,m}^{n+s+1} - \mathbf{U}_{l,m}^{n+s}) + C_h(\tilde{\mathbf{U}}^{n+s}, \widehat{\mathbf{U}}^{n+s+1})_{l,m} + \nu\Delta_{3h}\widehat{\mathbf{U}}_{l,m}^{n+s+1} + \mathbf{F}_{l,m}^{n+s+1}, \tag{47}$$

$$\frac{1}{\Delta t}(\mathbf{U}_{l,m}^{n+s+1} - \widehat{\mathbf{U}}_{l,m}^{n+s+1}) = -\nabla_{3h}^- P_{l,m}^{n+s+1}, \tag{48}$$

$$\nabla_{3h}^+ \cdot \mathbf{U}_{l,m}^{n+s+1} = 0, \tag{49}$$

$$\mathbf{U}_{l,0}^{n+m+1} = \mathbf{U}_{N_1+1,m}^{n+s+1} = \mathbf{U}_{l,N_2+1}^{n+s+1} = \mathbf{U}_{0,m}^{n+s+1} = 0, \tag{50}$$

where $i = 1, \ldots, 3N_1, j = 1, \ldots, 3N_2, l = 1, \ldots, N_1,$, $m = 1, \ldots, N_2$ and $\widehat{\mathbf{u}}$ and $\widehat{\mathbf{U}}$ are temporary non-divergence-free velocity fields on the fine mesh and coarse mesh, respectively.

We split the full equation by first computing the velocity field without considering the pressure, (42), and then adding the pressure, (43). Combining equations (42) and (43), we obtain a numerical approximation to equation (2) on the fine mesh. We first compute (42) to determine the non-divergence free velocity $\widehat{\mathbf{u}}_{i,j}^{n+(r+1)/\tau}$; then using the divergence free condition on the final velocity field (44), the pressure is determined from (43). By taking the divergence of (43) and using (44), we obtain a Poisson equation for the pressure:

$$\Delta_h p_{i,j}^{n+(r+1)/\tau} = \frac{\tau}{\Delta t} \nabla_h \cdot \widehat{\mathbf{u}}_{i,j}^{n+(r+1)/\tau}. \tag{51}$$

From (51), the pressure $p_{i,j}^{n+(r+1)/\tau}$ in the projection method satisfies the artificial Neumann boundary condition $\left.\frac{\partial p}{\partial n}\right|_{\partial\Omega} = 0$, see [13, 14]. Hence, the boundary conditions for the pressure on the fine mesh are given by

$$p_{0,j} = p_{1,j}, \quad p_{3N_1+1,j} = p_{3N_1,j}, \quad p_{i,0} = p_{1,j}, \quad p_{i,3N_2+1} = p_{i,3N_2}, \tag{52}$$

for $i = 1, \ldots, 3N_1$ and $j = 1, \ldots, 3N_2$. The boundary conditions of the pressure on the coarse mesh are defined in a similar way.

Once the pressure has been found, the final velocity field is obtained from (43). The same procedure applies on (48) and (49) to find the final velocity field and pressure on the coarse mesh.

Theorem 4.1. *The finite volume discretization* (42)-(50) *is conditionally stable; that is, for* $\Delta t \leq \frac{1}{2\eta}$,

$$\|\boldsymbol{u}^n\|_h^2 \leq 2^{2T\eta}\Big[\,\|\boldsymbol{u}^0\|_h^2 + T\eta M\Big], \tag{53}$$

where $M = \max_n \|f^n\|_h$ *and* $\eta = \left(1 - \frac{2\nu}{c_0}\right)$.

Proof: To prove this result we use the energy method. First taking the scalar product of (42) with $\frac{2}{\tau}\Delta t \Delta x \Delta y\, \widehat{\mathbf{u}}_{i,j}^{n+(r+1)/\tau}$ and taking the sum, we obtain

$$\begin{aligned}
&2(\widehat{\mathbf{u}}^{n+(r+1)/\tau} - \mathbf{u}^{n+r/\tau}, \widehat{\mathbf{u}}^{n+(r+1)/\tau})_h \\
=&\frac{2\Delta t}{\tau}\nu(\widehat{\mathbf{u}}^{n+(r+1)/\tau}, \Delta_h \widehat{\mathbf{u}}^{n+(r+1)/\tau})_h + \frac{2\Delta t}{\tau}(\mathbf{f}^{n+(r+1)/\tau}, \widehat{\mathbf{u}}^{n+(r+1)/\tau})_h \\
=&-\frac{2\Delta t}{\tau}\nu(\nabla_h \widehat{\mathbf{u}}^{n+(r+1)/\tau}, \nabla_h \widehat{\mathbf{u}}^{n+(r+1)/\tau})_h + \frac{2\Delta t}{\tau}(\mathbf{f}^{n+(r+1)/\tau}, \widehat{\mathbf{u}}^{n+(r+1)/\tau})_h \\
=&-\frac{2\Delta t\,\nu}{\tau}|\widehat{\mathbf{u}}^{n+(r+1)/\tau}|_{1,h}^2 + \frac{2\Delta t}{\tau}(\mathbf{f}^{n+(r+1)/\tau}, \widehat{\mathbf{u}}^{n+(r+1)/\tau})_h.
\end{aligned} \tag{54}$$

Using (24), (26) and Young's inequality, equation (54) gives

$$\begin{aligned}
&\left[1 + \frac{\Delta t}{\tau}\left(\frac{2\nu}{c_0} - 1\right)\right]\|\widehat{\mathbf{u}}^{n+(r+1)/\tau}\|_h^2 - \|\mathbf{u}^{n+r/\tau}\|_h^2 + \|\widehat{\mathbf{u}}^{n+(r+1)/\tau} - \mathbf{u}^{n+r/\tau}\|_h^2 \\
\leq&\frac{\Delta t}{\tau}\|\mathbf{f}^{n+(r+1)/\tau}\|_h^2.
\end{aligned} \tag{55}$$

Since $\mathbf{f}$ is a bounded function, we have

$$\|\mathbf{f}^{n+(r+1)/\tau}\|_h^2 \leq M_0,$$

where

$$M_0 = \sup_{t\in[0,T]} \|\mathbf{f}(x,y,t)\|.$$

Thus from (55) we have

$$\left[1 - \frac{\Delta t}{\tau}\left(1 - \frac{2\nu}{c_0}\right)\right] \|\widehat{\mathbf{u}}^{n+(r+1)/\tau}\|_h^2 - \|\mathbf{u}^{n+r/\tau}\|_h^2 \leq \frac{\Delta t}{\tau} M_0^2. \tag{56}$$

Based on (27) for

$$\Delta t \leq \frac{\tau}{2\eta}, \tag{57}$$

we have

$$\|\widehat{\mathbf{u}}^{n+(r+1)/\tau}\|_h^2 \leq 2^{\frac{2\Delta t\eta}{\tau}} \left[\|\mathbf{u}^{n+r/\tau}\|_h^2 + \frac{\Delta t}{\tau} M_0^2\right], \tag{58}$$

where $\eta = \left(1 - \dfrac{2\nu}{c_0}\right)$.

Multiplying (43) with $\dfrac{2}{\tau}\Delta t\Delta x\Delta y\, \mathbf{u}_{i,j}^{n+(r+1)/\tau}$ and summing, we get

$$\begin{aligned} \|\mathbf{u}^{n+(r+1)/\tau}\|_h^2 - \|\widehat{\mathbf{u}}^{n+(r+1)/\tau}\|_h^2 + &\qquad \|\mathbf{u}^{n+(r+1)/\tau} - \widehat{\mathbf{u}}^{n+(r+1)/\tau}\|_h^2 \\ = -\frac{2\Delta t}{\tau}(\nabla_h \boldsymbol{p}^{n+(r+1)/\tau}, \mathbf{u}^{n+(r+1)/\tau})_h & \\ = \frac{2\Delta t}{\tau}(\boldsymbol{p}^{n+(r+1)/\tau}, \nabla_h \cdot \mathbf{u}^{n+(r+1)/\tau})_h. & \end{aligned} \tag{59}$$

Applying (43), (59) yields

$$\|\mathbf{u}^{n+(r+1)/\tau}\|_h \leq \|\widehat{\mathbf{u}}^{n+(r+1)/\tau}\|_h. \tag{60}$$

Combining (58) and (60), we get

$$\|\mathbf{u}^{n+(r+1)/\tau}\|_h^2 \leq 2^{\frac{2\Delta t\eta}{\tau}} \left[\|\mathbf{u}^{n+r/\tau}\|_h^2 + \frac{\Delta t}{\tau} M_0^2\right].$$

After τ iterations, we obtain

$$\begin{aligned} \|\mathbf{u}^{n+1}\|_h^2 &\leq 2^{\frac{2\Delta t\,\eta}{\varepsilon^2}} \|\mathbf{u}^n\|_h^2 + \frac{\Delta t M_0^2}{\tau}\left[\sum_{j=1}^{\tau}\left(2^{\frac{2\Delta t\,j\,\eta}{\tau}}\right)\right] \\ &\leq 2^{2\Delta t\,\eta}\Big[\|\mathbf{u}^n\|_h^2 + \Delta t M_0^2\Big]. \end{aligned} \tag{61}$$

We now perform q iterations on the coarse grid, (47), using time step Δt and the relations (41). At time $t_{n+s} = (n+s)\Delta t, 2 \leq s \leq q+1$, the incremental unknowns $\mathbf{Z}_{i,j}$ are frozen at time $(n+1)\Delta t$. As in the case on the fine mesh, taking the scalar product of (47) with $18\Delta t\Delta x\Delta y\, \widehat{\mathbf{U}}_{l,m}^{n+s+1}$ and adding the equalities for $l = 1, \ldots, N_1$ and $m = 1, \ldots, N_2$, together with (24), (26) and Young's inequality, we obtain

$$[1 - \Delta t\,\eta]\, \|\widehat{\mathbf{U}}^{n+s+1}\|_{3h}^2 - \|\mathbf{U}^{n+s}\|_{3h}^2 \leq \Delta t\, M_0^2. \tag{62}$$

Using (27) for

$$\Delta t \leq \frac{1}{2\eta}, \tag{63}$$

(62) gives

$$\|\widehat{\mathbf{U}}^{n+s+1}\|_{3h}^2 \leq 2^{2\Delta t\,\eta}\Big[\|\mathbf{U}^{n+s}\|_{3h}^2 + \Delta t\, M_0^2\Big]. \tag{64}$$

Using (64) and the fact that $\|\mathbf{U}^{n+s+1}\|_{3h}^2 \leq \|\widehat{\mathbf{U}}^{n+s+1}\|_{3h}^2$, we get

$$\|\mathbf{U}^{n+s+1}\|_{3h}^2 \leq 2^{2\Delta t\,\eta}\Big[\|\mathbf{U}^{n+s}\|_{3h}^2 + \Delta t\, M_0^2\Big]. \tag{65}$$

From the definition of the increments $\mathbf{Z}^{n+1}_{3l-\alpha,3m-\beta}$, we have

$$\mathbf{u}^{n+s}_{3l-\alpha,3m-\beta} = \mathbf{U}^{n+s}_{l,m} + \mathbf{Z}^{n+1}_{3l-\alpha,3m-\beta}, \quad 1 \leq l \leq N_1, 1 \leq m \leq N_2, \quad \alpha,\beta = 0,1,2.$$

Taking the sum over α and β, we get

$$\sum_{\alpha,\beta=0}^{2} |\mathbf{u}^{n+s}_{3l-\alpha,3m-\beta}|^2 = \sum_{\alpha,\beta=0}^{2} |\mathbf{U}^{n+s}_{l,m} + \mathbf{Z}^{n+1}_{3l-\alpha,3m-\beta}|^2 = 9|\mathbf{U}^{n+s}_{l,m}|^2 + \sum_{\alpha,\beta=0}^{2} |\mathbf{Z}^{n+1}_{3l-\alpha,3m-\beta}|^2,$$

where $|.|$ is an Euclidean norm in 2D. For $s = 1, \ldots, q+1$, the following relation holds:

$$\|\mathbf{u}^{n+s}\|_h^2 = \|\mathbf{U}^{n+s}\|_{3h}^2 + \|\mathbf{Z}^{n+1}\|_h^2. \tag{66}$$

By adding $\|\mathbf{Z}^{n+1}\|_h^2$ to both sides of inequality (65) and using (66), we get

$$\|\mathbf{u}^{n+s+1}\|_h^2 \leq 2^{2\Delta t\,\eta}\Big[\|\mathbf{u}^{n+s}\|_h^2 + \Delta t\, M_0^2\Big].$$

After q iterations, and using (61), we have

$$\|\mathbf{u}^{n+q+1}\|_h^2 \leq 2^{2\Delta t\,(q+1)\,\eta}\Big[\|\mathbf{u}^{n}\|_h^2 + \Delta t(q+1)\, M_0^2\Big].$$

By induction over n, we obtain

$$\begin{aligned}\|\mathbf{u}^{n}\|_h^2 &\leq 2^{2\Delta t n\eta}\Big[\|\mathbf{u}^{0}\|_h^2 + \Delta t n M_0^2\Big]\\ &\leq 2^{2T\eta}\Big[\|\mathbf{u}^{0}\|_h^2 + T M_0^2\Big]\end{aligned}$$

This completes the proof. □

Remark 4.1. *From* (56) *and* (62), *for big enough ν, that is for $\nu \geq \frac{c_0}{2}$, we have*

$$\|\boldsymbol{u}^n\|_h^2 \leq \|\boldsymbol{u}^0\|_h^2 + \Delta t n M_0^2 \leq \|\boldsymbol{u}^0\|_h^2 + T M_0^2,$$

for $n = 1, \ldots, M$.

Remark 4.2. *The conditions for the stability of the implicit multilevel finite volume method are given in* (57) *and* (63). *This shows that the method is more restricted on the coarse mesh than the fine mesh.*

5. Explicit method

In this section, we consider the projection method of [9] to discretize (2) using explicit multilevel finite volume schemes where the convective term is approximated by

$$(\mathbf{u}\cdot\nabla)\mathbf{u}\Big|_{t=(n+1)\Delta t} \approx C_h(\mathbf{u}^n,\mathbf{u}^n),$$

and the approximations on the fine and coarse meshes are obtained similarly.

For $0 \le r \le \tau - 1$ and $1 \le s \le q$, we discretize (2) using explicit multilevel finite volume method.

$$\begin{aligned}
&\frac{\tau}{\Delta t}(\widehat{\mathbf{u}}_{i,j}^{n+(r+1)/\tau} - \mathbf{u}_{i,j}^{n+r/\tau}) + (C_h(\mathbf{u}^{n+r/\tau},\mathbf{u}^{n+r/\tau}))_{i,j} \\
&\qquad\qquad = \nu\Delta_h \mathbf{u}_{i,j}^{n+r/\tau} + \mathbf{f}_{i,j}^{n+r/\tau}, && \text{(67a)}\\
&\frac{\tau}{\Delta t}(\mathbf{u}_{i,j}^{n+(t+1)/\tau} - \widehat{\mathbf{u}}_{i,j}^{n+(r+1)/\tau}) = -\nabla_h^- p_{i,j}^{n+(r+1)/\tau}, && \text{(67b)}\\
&\nabla_h^+\cdot \mathbf{u}_{i,j}^{n+(r+1)/\tau} = 0, && \text{(67c)}\\
&\mathbf{u}_{0,j}^{n+r/\tau} = \mathbf{u}_{i,0}^{n+r/\tau} = \mathbf{u}_{3N_1+1,j}^{n+r/\tau} = \mathbf{u}_{i,3N_2+1}^{n+r/\tau} = 0, && \text{(67d)}\\
&\mathbf{u}_{i,j}^0 = \frac{1}{\Delta x\Delta y}\iint_{k_{i,j}} \mathbf{u}_0(x,y)\,dx\,dy, && \text{(67e)}\\
&\frac{1}{\Delta t}(\widehat{\mathbf{U}}_{l,m}^{n+s+1} - \mathbf{U}_{l,m}^{n+s}) - (C_{3h}(\mathbf{U}^{n+s},\mathbf{U}^{n+s}))_{l,m} = \nu\Delta_{3h}\mathbf{U}_{l,m}^{n+s} + \mathbf{F}_{l,m}^{n+s}. && \text{(67f)}\\
&\frac{1}{\Delta t}(\mathbf{U}_{l,m}^{n+s+1} - \widehat{\mathbf{U}}_{l,m}^{n+s+1}) = -\nabla_{3h}^- P_{l,m}^{n+s+1}, && \text{(67g)}\\
&\nabla_{3h}^+\cdot \mathbf{U}_{l,m}^{n+s+1} = 0, && \text{(67h)}\\
&\mathbf{U}_{0,m}^{n+s} = \mathbf{U}_{l,0}^{n+s} = \mathbf{U}_{N_1+1,m}^{n+s} = \mathbf{U}_{l,N_2+1}^{n+s} = 0, && \text{(67i)}
\end{aligned}$$

where $1 \le i \le 3N_1$, $1 \le l \le N_1$, $1 \le j \le 3N_2$ and $1 \le m \le N_2$. The pressure is associated with homogeneous Neumann boundary condition.

Theorem 5.1. *We assume that the following are satisfied for some δ, $0 < \delta < 1$:*

$$16\Delta t\left(\frac{1}{\Delta x^2} + \frac{1}{\Delta y^2}\right) \le \frac{1-\delta}{\nu}\min\{\tau, 9\}, \tag{68}$$

$$\frac{72\Delta t}{\Delta x\,\Delta y}\Big(|\alpha_1| + |\alpha_2|\Big)^2 \le \frac{\nu\delta}{2D}\min\{\tau, 9\}. \tag{69}$$

Then the multilevel method defined by the equations (67a)-(67i) *is* $L^\infty(0,T;\mathcal{H}_h)$ *stable in the sense that*

$$\|\boldsymbol{u}^n\|_h^2 \le D, \quad n = 1, 2\ldots, M,$$

where

$$D = \|\boldsymbol{u}_0\|_h^2 + T\left(\frac{c_0^2}{\nu} + 2T\right)\|\boldsymbol{f}\|_h,$$

$\|\boldsymbol{f}\|_h = \max\limits_n \|\boldsymbol{f}^n\|_h$.

Proof. To prove this result we use once again the energy method. We assume n is a multiple of $q+1$. Taking the scalar product in $\mathcal{H}_h$ of (67a) with $\dfrac{2\Delta t\,\Delta x\,\Delta y}{\tau}\,\widehat{\mathbf{u}}_{i,j}^{n+r/\tau}$

and taking the sum for $i = 1, \dots, 3N_1$ and $j = 1, \dots, 3N_2$, we obtain

$$\begin{aligned} &\|\widehat{\mathbf{u}}^{n+(r+1)/\tau}\|_h^2 - \|\mathbf{u}^{n+r/\tau}\|_h^2 - \|\widehat{\mathbf{u}}^{n+(r+1)/\tau} - \mathbf{u}^{n+r/\tau}\|_h^2 + \frac{2\Delta t\nu}{\tau}|\mathbf{u}^{n+r/\tau}|_{1,h}^2 \\ &= \frac{2\Delta t}{\tau}(\mathbf{u}^{n+r/\tau}, \mathbf{f}^{n+r/\tau})_h. \end{aligned} \tag{70}$$

Eq. (70) together with (25) and (26) gives

$$\begin{aligned} &\|\widehat{\mathbf{u}}^{n+(r+1)/\tau}\|_h^2 - \|\mathbf{u}^{n+r/\tau}\|_h^2 - \|\widehat{\mathbf{u}}^{n+(r+1)/\tau} - \mathbf{u}^{n+r/\tau}\|_h^2 + \frac{\Delta t\nu}{\tau}|\mathbf{u}^{n+r/\tau}|_{1,h}^2 \\ &\leq \frac{\Delta t c_0^2}{\tau}\|\mathbf{f}^{n+r/\tau}\|_h. \end{aligned} \tag{71}$$

To estimate the term $\|\widehat{\mathbf{u}}^{n+(r+1)/\tau} - \mathbf{u}^{n+r/\tau}\|_h^2$, we take the scalar product in $\mathcal{H}_h$ (67a) with $\dfrac{2\Delta t\Delta x\Delta y}{\tau}(\widehat{\mathbf{u}}_{i,j}^{n+(r+1)/\tau} - \mathbf{u}_{i,j}^{n+r/\tau})$ and sum from $i = 1$ to $i = 3N_1$ and from $j = 1$ to $j = 3N_2$, then gives

$$\begin{aligned} 2\|\widehat{\mathbf{u}}^{n+(r+1)/\tau} - \mathbf{u}^{n+r/\tau}\|_h^2 =& -\frac{2\Delta t}{\tau}(C_h(\mathbf{u}^{n+r/\tau}, \mathbf{u}^{n+r/\tau}), \widehat{\mathbf{u}}^{n+(r+1)/\tau} - \mathbf{u}^{n+r/\tau}) \\ &+ \frac{2\Delta t\nu}{\tau}(\Delta_h \mathbf{u}^{n+r/\tau}, \widehat{\mathbf{u}}^{n+(r+1)/\tau} - \mathbf{u}^{n+r/\tau})_h \\ &+ \frac{2\Delta t}{\tau}(\mathbf{f}^{n+r/\tau}, \widehat{\mathbf{u}}^{n+(r+1)/\tau} - \mathbf{u}^{n+r/\tau})_h \\ \leq& \frac{2\Delta t}{\tau}|(C_h(\mathbf{u}^{n+r/\tau}, \mathbf{u}^{n+r/\tau}), \widehat{\mathbf{u}}^{n+(r+1)/\tau} - \mathbf{u}^{n+r/\tau})_h| \\ &+ \frac{2\Delta t\nu}{\tau}|\mathbf{u}^{n+r/\tau}|_{1,h}\, |\widehat{\mathbf{u}}^{n+(r+1)/\tau} - \mathbf{u}^{n+r/\tau}|_{1,h} \\ &+ \frac{2\Delta t}{\tau}\|\mathbf{f}^{n+r/\tau}\|_h\, \|\widehat{\mathbf{u}}^{n+(r+1)/\tau} - \mathbf{u}^{n+r/\tau}\|_h. \end{aligned}$$

Using (22), (23), Young's inequality and Lemma 2.2, we have

$$\begin{aligned} &\frac{2\Delta t\nu}{\tau}|(C_h(\mathbf{u}^{n+r/\tau}, \mathbf{u}^{n+r/\tau}), \widehat{\mathbf{u}}^{n+(r+1)/\tau} - \mathbf{u}^{n+r/\tau})_h| \\ \leq& \frac{6\Delta t\sqrt{2}}{\tau}\Big(|\alpha_1| + |\alpha_2|\Big)\|\mathbf{u}^{n+r/\tau}\|_{h,\infty}|\mathbf{u}^{n+r/\tau}|_{1,h}\|\widehat{\mathbf{u}}^{n+(r+1)/\tau} - \mathbf{u}^{n+r/\tau}\|_h \\ \leq& \frac{72\Delta t^2}{\tau^2}\Big(|\alpha_1| + |\alpha_2|\Big)^2\|\mathbf{u}^{n+r/\tau}\|_{h,\infty}^2|\mathbf{u}^{n+r/\tau}|_{1,h}^2 + \frac{1}{4}\|\widehat{\mathbf{u}}^{n+(r+1)/\tau} - \mathbf{u}^{n+r/\tau}\|_h^2 \\ \leq& \frac{72\Delta t^2\,\gamma}{\Delta x\,\Delta y\,\tau^2}\|\mathbf{u}^{n+r/\tau}\|_h^2|\mathbf{u}^{n+r/\tau}|_{1,h}^2 + \frac{1}{4}\|\widehat{\mathbf{u}}^{n+(r+1)/\tau} - \mathbf{u}^{n+r/\tau}\|_h^2, \end{aligned}$$

and

$$\begin{aligned} &\frac{2\Delta t\nu}{\tau}|\mathbf{u}^{n+r/\tau}|_{1,h}\, |\widehat{\mathbf{u}}^{n+(r+1)/\tau} - \mathbf{u}^{n+r/\tau})_h|_{1,h} \\ \leq& \frac{4\Delta t\,\nu}{\tau}\left(\frac{1}{\Delta x^2} + \frac{1}{\Delta y^2}\right)^{1/2}\, |\mathbf{u}^{n+r/\tau}|_{1,h}\, \|\widehat{\mathbf{u}}^{n+(r+1)/\tau} - \mathbf{u}^{n+r/\tau}\|_h \\ \leq& \frac{16\Delta t^2\,\nu^2}{\tau^2}\left(\frac{1}{\Delta x^2} + \frac{1}{\Delta y^2}\right)\, |\mathbf{u}^{n+r/\tau}|_{1,h}^2 + \frac{1}{4}\|\widehat{\mathbf{u}}^{n+(r+1)/\tau} - \mathbf{u}^{n+r/\tau}\|_h, \end{aligned}$$

and

$$\frac{2\Delta t}{\tau}\|\mathbf{f}^{n+r/\tau}\|_h\, \|\widehat{\mathbf{u}}^{n+(r+1)/\tau} - \mathbf{u}^{n+r/\tau}\|_h \leq \frac{2\Delta t^2}{\tau^2}\|\mathbf{f}^{n+r/\tau}\|_h^2 + \frac{1}{2}\|\widehat{\mathbf{u}}^{n+(r+1)/\tau} - \mathbf{u}^{n+r/\tau}\|_h^2,$$

where $\gamma = \Big(|\alpha_1| + |\alpha_2|\Big)^2$, which yields

$$\|\widehat{\mathbf{u}}^{n+(r+1)/\tau} - \mathbf{u}^{n+r/\tau}\|_h^2 \leq \frac{16\Delta t^2\,\nu^2}{\tau^2}\left(\frac{1}{\Delta x^2} + \frac{1}{\Delta y^2}\right)|\mathbf{u}^{n+r/\tau}|_{1,h}^2 + \frac{72\Delta t^2\,\gamma}{\Delta x\,\Delta y\,\tau^2}\|\mathbf{u}^{n+r/\tau}\|_h^2|\mathbf{u}^{n+r/\tau}|_{1,h}^2 + \frac{\Delta t^2}{\tau^2}|\mathbf{f}^{n+r/\tau}|_h^2.$$

Using (68), we obtain

$$\|\widehat{\mathbf{u}}^{n+(r+1)/\tau} - \mathbf{u}^{n+r/\tau}\|_h^2 \leq \frac{\Delta t\,\nu(1-\delta)}{\tau}|\mathbf{u}^{n+r/\tau}|_{1,h}^2 + \frac{72\Delta t^2\,\gamma}{\Delta x\,\Delta y\,\tau^2}\|\mathbf{u}^{n+r/\tau}\|_h^2|\mathbf{u}^{n}|_{1,h}^2 + \frac{2\Delta t^2}{\tau^2}|\mathbf{f}^{n+r/\tau}|_h^2.$$

Going back to (71), we get

$$\begin{aligned}\|\widehat{\mathbf{u}}^{n+(r+1)/\tau}\|_h^2 - \|\mathbf{u}^{n+r/\tau}\|_h^2 + \frac{\Delta t}{\tau}\left(\nu\delta - \frac{72\Delta t\,\gamma}{\Delta x\,\Delta y\,\tau}\|\mathbf{u}^{n+r/\tau}\|_h^2\right)|\mathbf{u}^{n+r/\tau}|_{1,h}^2 &\leq \frac{\Delta t}{\tau}\left(\frac{c_0^2}{\nu} + 2\frac{\Delta t}{\tau}\right)\|\mathbf{f}^{n+r/\tau}\|_h^2\\ &\leq \frac{\Delta t}{\tau}\left(\frac{c_0^2}{\nu} + 2T\right)\|\mathbf{f}\|_h^2.\end{aligned}$$

Letting $D_0 = \left(\dfrac{c_0^2}{\nu} + 2T\right)\|\mathbf{f}\|_h^2$, we have

$$\|\widehat{\mathbf{u}}^{n+(r+1)/\tau}\|_h^2 - \|\mathbf{u}^{n+r/\tau}\|_h^2 + \frac{\Delta t}{\tau}\left(\nu\delta - \frac{72\Delta t\,\gamma}{\Delta x\,\Delta y\,\tau}\|\mathbf{u}^{n+r/\tau}\|_h^2\right)|\mathbf{u}^{n+r/\tau}|_{1,h}^2 \leq \frac{\Delta t}{\tau}D_0. \tag{72}$$

From (67b) and the divergence free property, the inequality (60) holds. Thus, from (72), we obtain

$$\|\mathbf{u}^{n+(r+1)/\tau}\|_h^2 - \|\mathbf{u}^{n+r/\tau}\|_h^2 + \frac{\Delta t}{\tau}\left(\nu\delta - \frac{72\Delta t\,\gamma}{\Delta x\,\Delta y\,\tau}\|\mathbf{u}^{n+r/\tau}\|_h^2\right)|\mathbf{u}^{n+r/\tau}|_{1,h}^2 \leq \frac{\Delta t}{\tau}D_0. \tag{73}$$

In a similar fashion, from (67f) together with the assumption (68), we obtain

$$\|\mathbf{U}^{n+s+1}\|_{3h}^2 - \|\mathbf{U}^{n+s}\|_{3h}^2 + \Delta t\left(\nu\delta - \frac{8\Delta t\,\gamma}{\Delta x\,\Delta y}\|\mathbf{U}^{n+s}\|_{3h}^2\right)|\mathbf{U}^{n+s}|_{1,3h}^2 \leq \Delta t\,D_0. \tag{74}$$

Now we need to prove the following by induction on n:

$$\|\mathbf{u}^{n+(r+1)/\tau}\|_h^2 + \frac{\Delta t\,\nu\delta}{2\tau}|\mathbf{u}^{n+r/\tau}|_{1,h}^2 \leq \|\mathbf{u}^{n+r/\tau}\|_h^2 + \frac{\Delta t}{\tau}D_0, \quad \text{for } r = 0, 1, \dots, \tau-1, \tag{75}$$

$$\|\mathbf{U}^{n+s+1}\|_{3h}^2 + \frac{\Delta t\,\nu\delta}{2}|\mathbf{U}^{n+s}|_{1,3h}^2 \leq \|\mathbf{U}^{n+s}\|_{3h}^2 + \Delta t D_0, \quad \text{for } s = 1, 2, \dots, q. \tag{76}$$

We first show (75) and (76) hold by induction on r and s when $n = 0$. We first show that

$$\|\mathbf{u}^1\|_h^2 + \frac{\Delta t\,\nu\delta}{2\tau}\sum_{r=0}^{\tau-1}|\mathbf{u}^{r/\tau}|_{1,h}^2 \leq \|\mathbf{u}^0\|_h^2 + \Delta t D_0. \tag{77}$$

For $n = 0$, the relation (73) becomes

$$\|\mathbf{u}^{(r+1)/\tau}\|_h^2 - \|\mathbf{u}^{r/\tau}\|_h^2 + \frac{\Delta t}{\tau}\left(\nu\delta - \frac{72\Delta t\,\gamma}{\Delta x\,\Delta y\,\tau}\|\mathbf{u}^{r/\tau}\|_h^2\right)|\mathbf{u}^{r/\tau}|_{1,h}^2 \le \frac{\Delta t}{\tau}D_0. \tag{78}$$

For $r = 0$ using (69), we get

$$\begin{aligned}\|\mathbf{u}^{1/\tau}\|_h^2 + \frac{\Delta t\,\nu\delta}{\tau}|\mathbf{u}^0|_{1,h}^2 &\le \|\mathbf{u}^0\|_h^2 + \frac{\Delta t}{\tau}D_0 + \frac{72\Delta t^2\,\gamma}{\Delta x\,\Delta y\,\tau^2}\|\mathbf{u}^0\|_h^2|\mathbf{u}^0|_{1,h}^2\\ &\le \|\mathbf{u}^0\|_h^2 + \frac{\Delta t}{\tau}D_0 + \frac{\Delta t}{\tau}\frac{\nu\delta}{2}|\mathbf{u}^0|_{1,h}^2,\end{aligned}$$

which gives

$$\|\mathbf{u}^{1/\tau}\|_h^2 + \frac{\Delta t\,\nu\delta}{2\tau}|\mathbf{u}^0|_{1,h}^2 \le \|\mathbf{u}^0\|_h^2 + \frac{\Delta t}{\tau}D_0.$$

Let us assume that (77) holds up to $r-1$. From the assumption for $s = 1, 2, \ldots, r-1$, we have

$$\|\mathbf{u}^{s/\tau}\|_h^2 \le \|\mathbf{u}^0\|_h^2 + \frac{s\Delta t}{\tau}D_0 \le D.$$

The relation (78) becomes

$$\begin{aligned}\|\mathbf{u}^{(r+1)/\tau}\|_h^2 + \frac{\Delta t\,\nu\delta}{\tau}|\mathbf{u}^{r/\tau}|_{1,h}^2 &\le \|\mathbf{u}^{r/\tau}\|_h^2 + \frac{\Delta t}{\tau}\frac{72\Delta t\,\gamma}{\Delta x\,\Delta y\,\tau}\|\mathbf{u}^{r/\tau}\|_h^2|\mathbf{u}^{r/\tau}|_{1,h}^2 + \frac{\Delta t}{\tau}D_0\\ &\le \|\mathbf{u}^{r/\tau}\|_h^2 + \frac{\Delta t\nu\delta}{2\tau}|\mathbf{u}^{r/\tau}|_{1,h}^2 + \frac{\Delta t}{\tau}D_0 \end{aligned} \tag{79}$$

which shows us that (75) is true for $n = 0$. From (79), we have

$$\|\mathbf{u}^1\|_h^2 + \frac{\Delta t\,\nu\delta}{2\tau}\sum_{r=0}^{\tau-1}|\mathbf{u}^{r/\tau}|_{1,h}^2 \le \|\mathbf{u}^0\|_h^2 + \Delta t D_0,$$

which implies

$$\|\mathbf{u}^1\|_h^2 \le \|\mathbf{u}^0\|_h^2 + \Delta t D_0. \tag{80}$$

We then show (76) by using induction on s for $n = 0$. From the definition of $\mathbf{U}$, we have

$$\|\mathbf{U}^n\|_{3h}^2 \le \|\mathbf{u}^n\|_h^2. \tag{81}$$

For $s = 1$, from (74), we have

$$\|\mathbf{U}^2\|_{3h}^2 - \|\mathbf{U}^1\|_{3h}^2 + \Delta t\left(\nu\delta - \frac{8\Delta t\,\gamma}{\Delta x\,\Delta y}\|\mathbf{U}^1\|_{3h}^2\right)|\mathbf{U}^1|_{1,3h}^2 \le \Delta t\,D_0.$$

Then using (80) and (81) together with (69), we arrive at

$$\|\mathbf{U}^2\|_{3h}^2 + \frac{\Delta t\,\nu\delta}{2}|\mathbf{U}^1|_{1,3h}^2 \le \|\mathbf{U}^1\|_{3h}^2 + \Delta t D_0.$$

We now assume that (76) holds true up to the order $q-1$; that is,

$$\|\mathbf{U}^{s+1}\|_{3h}^2 + \frac{\Delta t\,\nu\delta}{2}|\mathbf{U}^s|_{1,3h}^2 \le \|\mathbf{U}^s\|_{3h}^2 + \Delta t D_0 \text{ for } s = 1, \ldots, q-1,$$

and we observe that

$$\|\mathbf{U}^{s+1}\|_{3h}^2 \le \|\mathbf{U}^s\|_{3h}^2 + \Delta t D_0 \le D, \text{ for } s = 1, \ldots, q-1. \tag{82}$$

From (74) and (82) together with (69) we obtain the result. Thus using (41) and (66), we find that

$$\|\mathbf{u}^{s+1}\|_h^2 \le D, \text{ for } s = 0, \ldots, q.$$

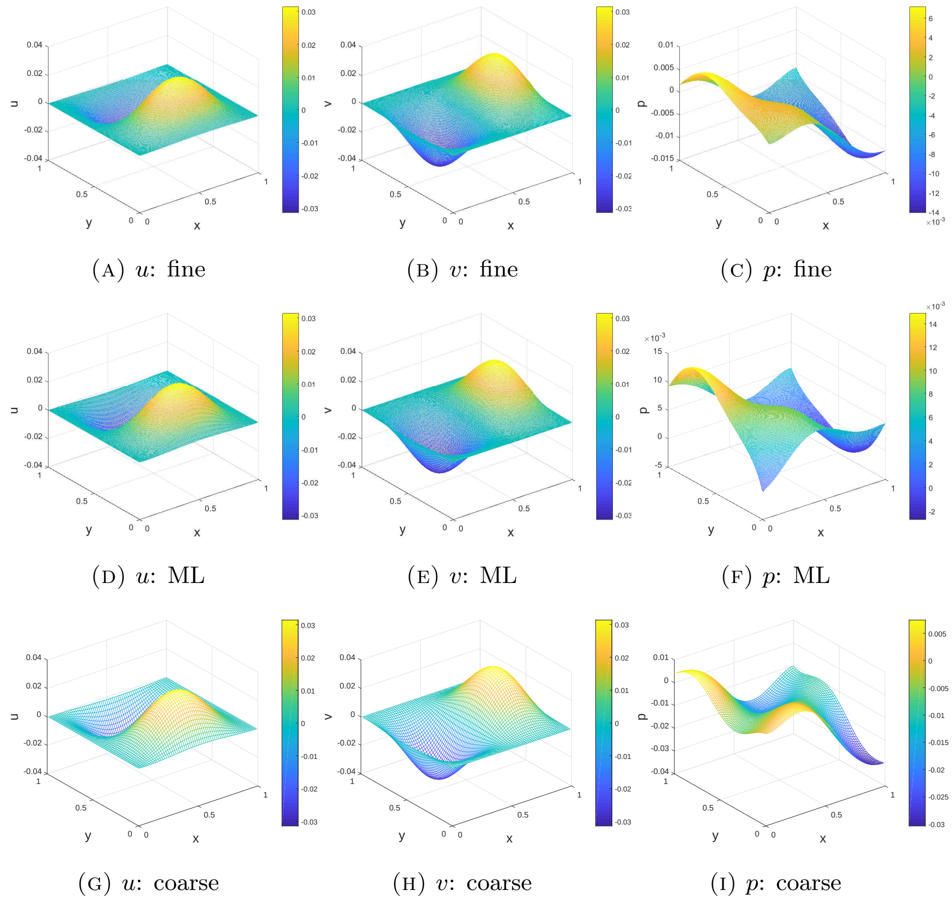

(A) u: fine (B) v: fine (C) p: fine

(D) u: ML (E) v: ML (F) p: ML

(G) u: coarse (H) v: coarse (I) p: coarse

FIGURE 1. Velocities and pressure obtained from implicit methods for $N = 64$ and $\Delta t = 0.0001$ at $T = 0.01$ for Example 1.

Using the same approach as in the case $n = 0$, it can be easily proved by induction on r and s. Hence, (75) and (76) hold for any $n = z(q + 1)$, where z is a positive integer. Therefore, the proof is complete. □

6. Numerical results

In this section, we present the numerical results of the multilevel finite volume methods developed for the 2D incompressible Navier-Stokes equations defined on a unit square domain $\Omega = [0, 1] \times [0, 1]$. The multilevel finite volume methods are compared with the respective traditional one-level finite volume methods on the fine and coarse meshes. For the traditional one-level methods on the fine mesh, we use the time step $\Delta t/p$ and spatial step sizes $\Delta x = \Delta y$, that is $N_1 = N_2 = N$, and the one-level methods on the coarse mesh, we use the time step size Δt and spatial step sizes $3\Delta x = 3\Delta y$. In the following, we refer the one-level methods on the fine mesh as "fine", one-level methods on the coarse mesh as "coarse" and multilevel methods as "ML".

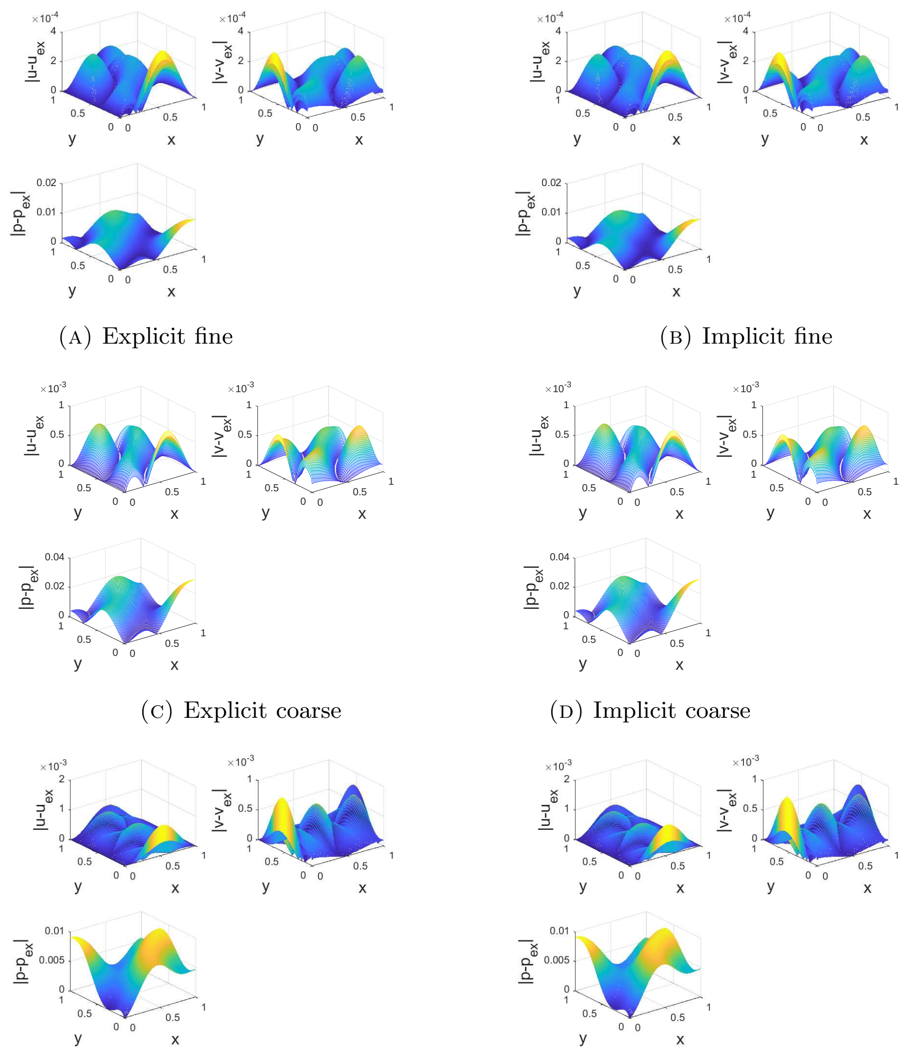

(A) Explicit fine (B) Implicit fine

(C) Explicit coarse (D) Implicit coarse

(E) Explicit ML (F) Implicit ML

FIGURE 2. Absolute error fields of Example 1 for $N = 64$ and $\Delta t = 0.0001$ at $T = 0.01$.

We consider three numerical examples. For each example different uniform grid sizes are used for some time step sizes where the viscosity coefficient is chosen as $\nu = 0.01$. The other parameters used for all the numerical results presented here are $\alpha_1 = \alpha_2 = \frac{1}{6}$, $p = 5$, and $q = 8$.

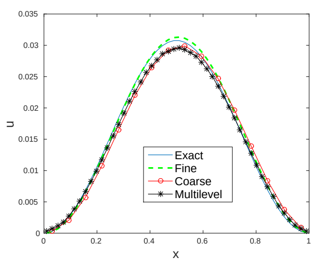

(A) u at $y = 0.2812$

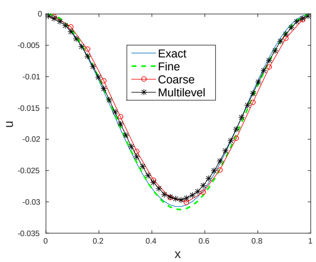

(B) u at $y = 0.7812$

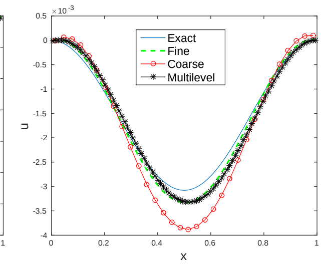

(C) u at $y = 0.5312$

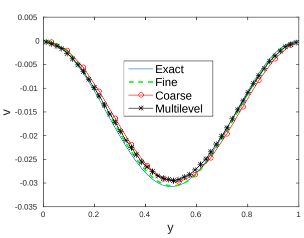

(D) v at $x = 0.2812$

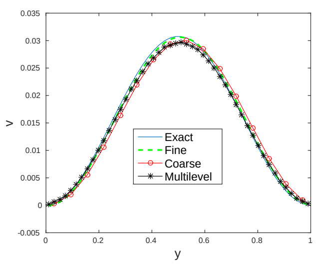

(E) v at $x = 0.7812$

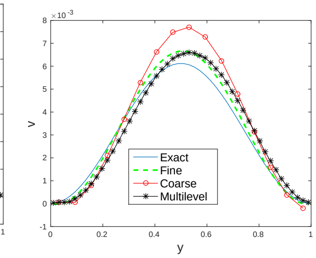

(F) v at $x = 0.5312$

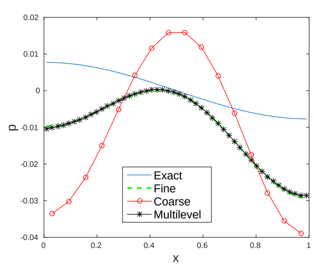

(G) p at $y = 0.2812$

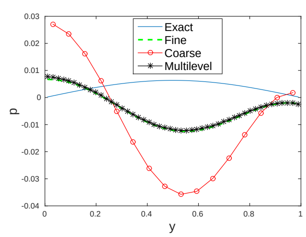

(H) p at $x = 0.2812$

FIGURE 3. Velocities and pressure obtained from explicit methods when $N = 16, \Delta t = 10^{-4}$ and $T = 0.01$ for some cell centres x and y Example 1.

The following error norms for the velocity and pressure are defined to evaluate the accuracy of the numerical methods:

$$L_u^2\text{-error} = \sqrt{\Delta x\, \Delta y \sum_{i=1}^{N} \sum_{j=1}^{N} \Big[\big(u_{i,j}^M - u(x_i, y_j, T)\big)^2 + \big(u_{i,j}^M - u(x_i, y_j, T)\big)^2 \Big]};$$

$$L_p^2\text{-error} = \sqrt{\Delta x\, \Delta y \sum_{i=1}^{N} \sum_{j=1}^{N} \big(p_{i,j}^M - p(x_i, y_j, T)\big)^2}.$$

The approximations of the convective term for the implicit method are given as follows [2]:

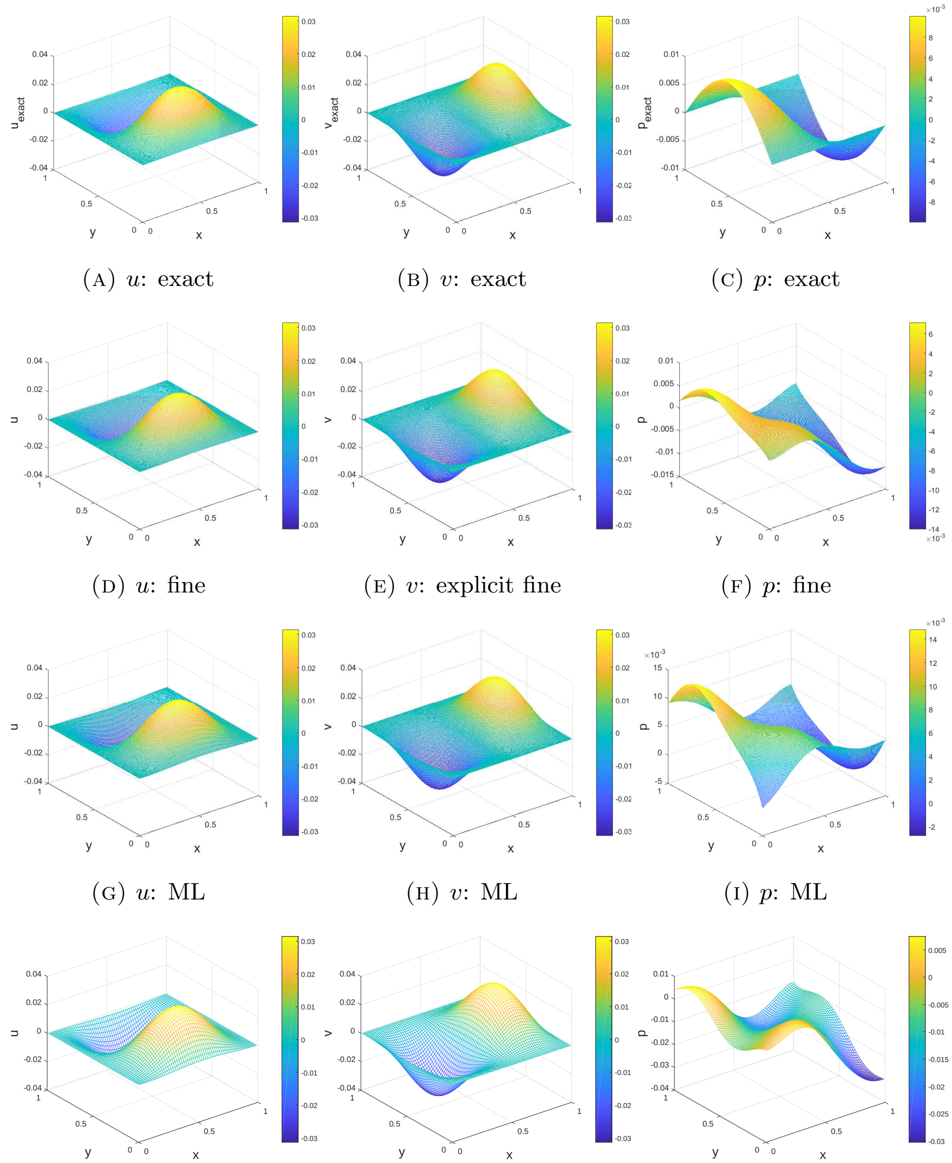

(A) u: exact (B) v: exact (C) p: exact

(D) u: fine (E) v: explicit fine (F) p: fine

(G) u: ML (H) v: ML (I) p: ML

(J) u: coarse (K) v: coarse (L) p: coarse

FIGURE 4. Velocities and pressure profiles obtained from explicit methods for $N = 64$ and $\Delta t = 0.0001$ at $T = 0.01$ and their exact solutions for Example 1.

- For the implicit multilevel method, for a non-negative integer z and $n = z(q+1)$, we use the following approximations:

$$
\begin{aligned}
\tilde{\mathbf{u}}^{n+r/\tau} &= \frac{1}{2}\left(\mathbf{u}^{n+r/\tau} + \mathbf{u}^{n+(r-1)/\tau}\right), \text{ for } r = 1, \ldots, \tau - 1, \\
\tilde{\mathbf{u}}^{n} &= \mathbf{u}^{n}, \\
\tilde{\mathbf{U}}^{n+s} &= \frac{1}{2}\left(\mathbf{U}^{n+s} + \mathbf{U}^{n+s-1}\right), \text{ for } s = 1, \ldots, q.
\end{aligned}
$$

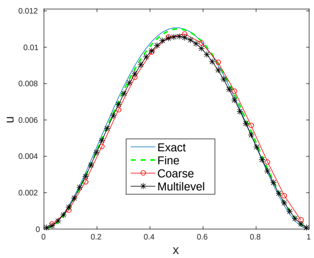

(A) explicit: u at y = 0.2812

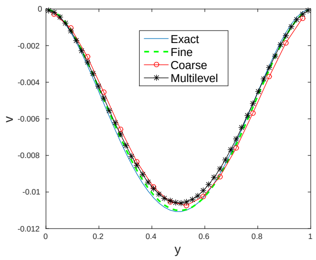

(B) explicit: v at x = 0.2812

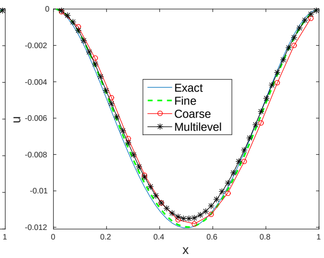

(C) explicit: u at y = 0.7812

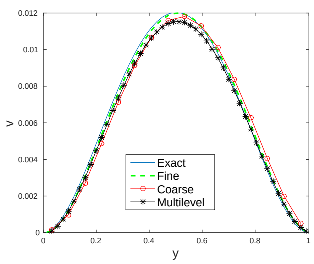

(D) explicit: v at x = 0.7812

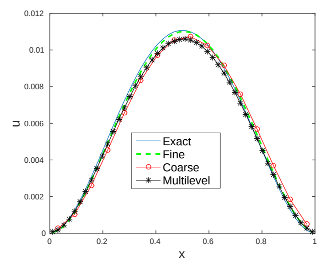

(E) implicit: u at y = 0.2812

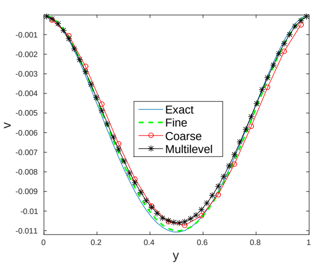

(F) implicit: v at x = 0.2812

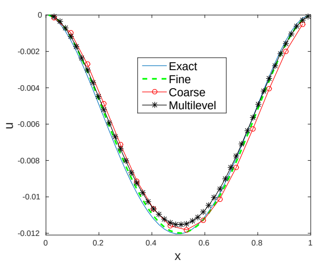

(G) implicit: u at y = 0.7812

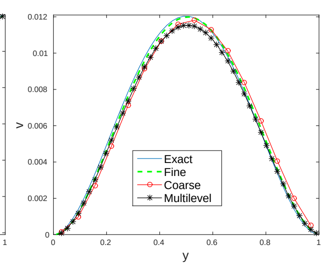

(H) implicit: v at x = 0.7812

FIGURE 5. Velocities when $\Delta t = 10^{-5}$ and $N = 16$ for some cell centres x and y at $T = 0.001$ for Example 2.

- For the implicit one-level method, $\tilde{\mathbf{u}}^n$ is approximated by the relation:

$$\tilde{\mathbf{u}}^n = \frac{1}{2}\left(\mathbf{u}^n + \mathbf{u}^{n-1}\right), \text{ for } n = 1, 2, \ldots, M-1.$$

- For both implicit methods we use $\tilde{\mathbf{u}}^0 = \mathbf{u}^0$.

Example 1

We consider the exact solutions [13]

$$u(x, y, t) = \pi \sin t \, \sin(2\pi y) \, \sin^2(\pi x) \tag{83}$$

$$v(x, y, t) = -\pi \sin t \, \sin(2\pi x) \, \sin^2(\pi y) \tag{84}$$

$$p(x, y, t) = \sin t \, \cos(\pi x) \, \sin(\pi y), \tag{85}$$

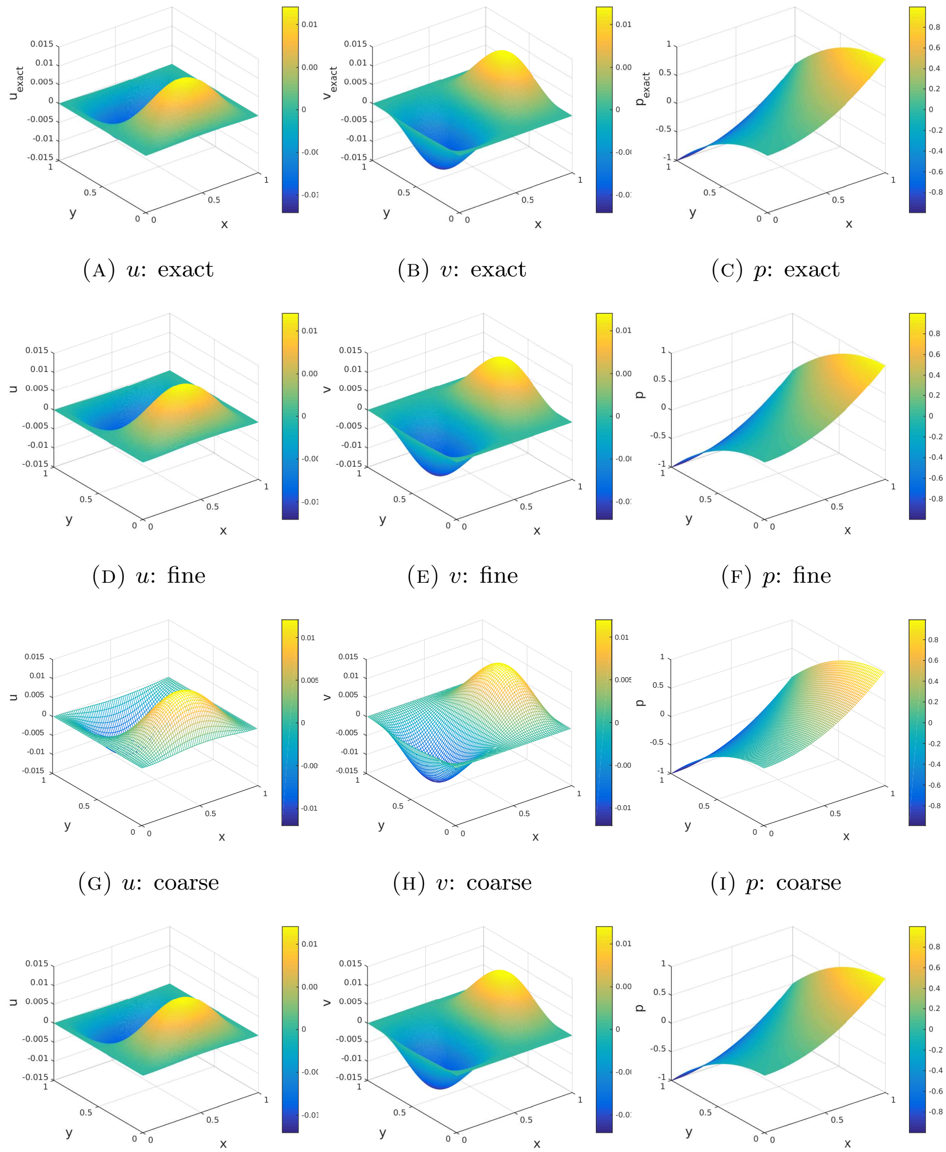

(A) u: exact (B) v: exact (C) p: exact

(D) u: fine (E) v: fine (F) p: fine

(G) u: coarse (H) v: coarse (I) p: coarse

(J) u: ML (K) v: ML (L) p: ML

FIGURE 6. Velocities and pressure obtained from explicit methods when $N = 64$ and $\Delta t = 10^{-4}$ at $T = 0.001$ and their exact profiles for Example 2.

where the source term is obtained on substitution to equation (2) and the initial condition for the velocity, $\mathbf{u}_0$, is obtained from (83) and (84) at $t = 0$.

Table 1 tabulates the errors and rates obtained from the numerical methods and the CPU time used to run each simulation at time $T = 0.01$. The 3D plots for the exact solutions and approximated solutions from the explicit and implicit methods are shown in Figures 4 and 1. In Figure 2, we show the velocities and pressure

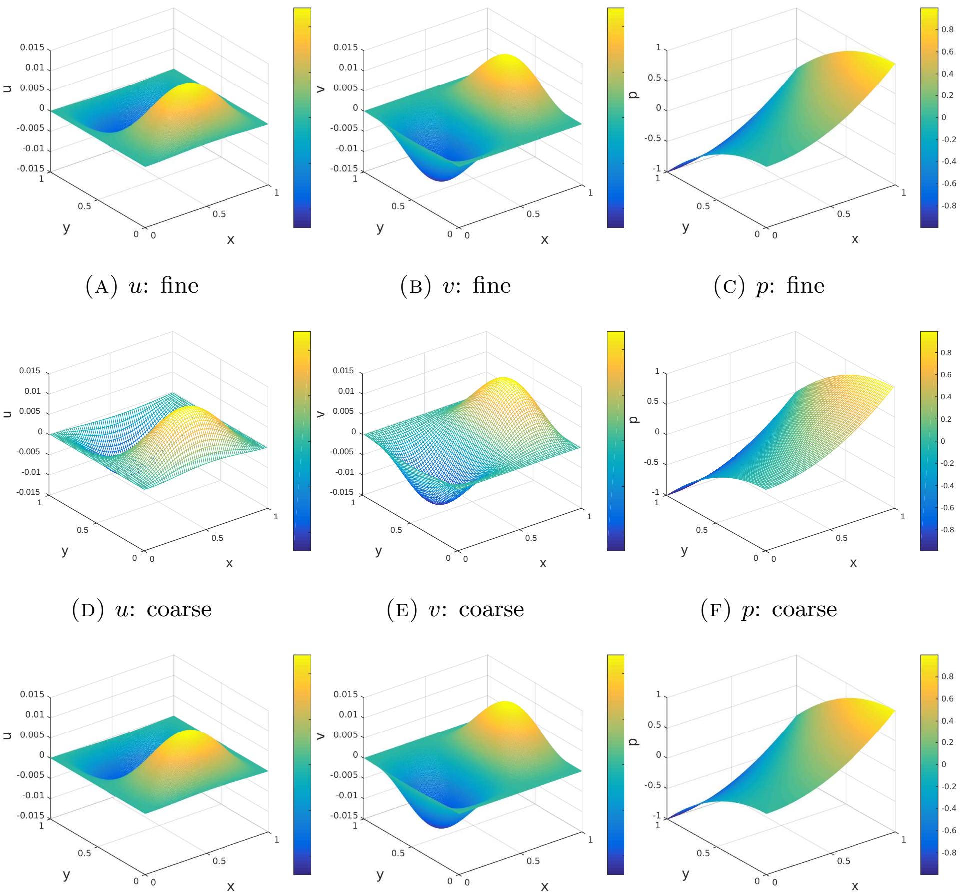

(A) u: fine (B) v: fine (C) p: fine

(D) u: coarse (E) v: coarse (F) p: coarse

(G) u: ML (H) v: ML (I) p: ML

FIGURE 7. Velocities and pressure obtained from implicit methods when $N = 64$ and $\Delta t = 10^{-4}$ at $T = 0.001$ for Example 2.

absolute error fields at $T = 0.01$ for time step $\Delta t = 0.0001$ with 64×64 mesh grid. Figure 3 shows the 2D plots of the velocities and pressure at some grid cells with peak velocity values.

From Table 1, we observe that the multilevel methods have better pressure approximation for $N = 16$ and $N = 32$ than the full one-level methods on fine and coarse mesh. It is also shown from Figures 3(g) and 3(h) at the cell centers $y = 0.2812$ and $x = 0.2812$, respectively, that the pressure obtained from the explicit multilevel method are in a good agreement with the results obtained from the one-level method on the fine mesh, while the pressure obtained from the one-level method on the coarse mesh is relatively far from the exact solution. For the approximation of the velocities, it is seen that the multilevel method works better for small space step, where the L^2_u-errors lie between the errors of the one-level methods. The 2D plots of the velocities at the peak values and at the cells next (right side) to the mid point are shown by Figures 3(a)-3(f). From these plots, we

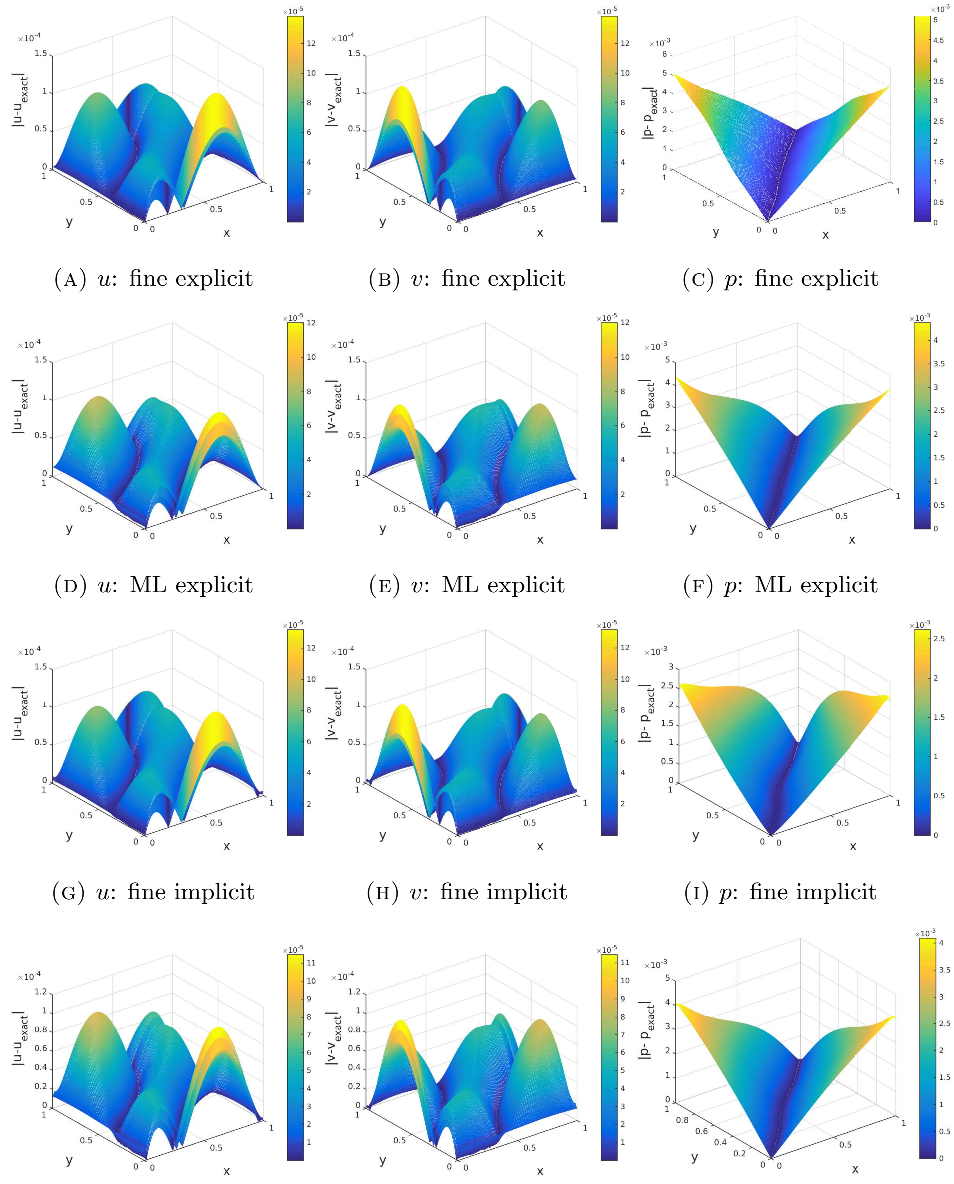

(A) u: fine explicit (B) v: fine explicit (C) p: fine explicit

(D) u: ML explicit (E) v: ML explicit (F) p: ML explicit

(G) u: fine implicit (H) v: fine implicit (I) p: fine implicit

(J) u: ML implicit (K) v: ML implicit (L) p: ML implicit

FIGURE 8. Absolute error fields of Example 2 when $N = 64$ and $\Delta t = 10^{-4}$ at $T = 0.001$.

observe that the velocities obtained from the multilevel method lies between the results from the one-level methods on the fine and coarse meshes.

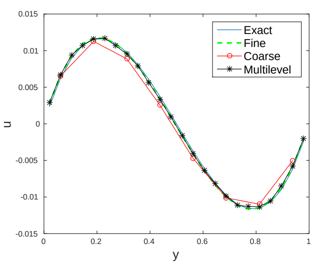

(A) u: $N = 8, x = 0.5625$

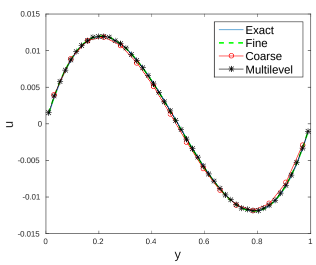

(B) u: $N = 16, x = 0.5312$

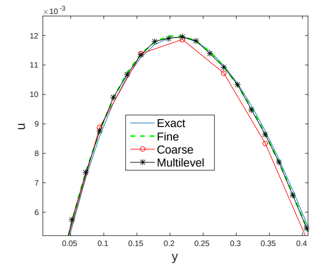

(C) Zoomed in (left 9(b))

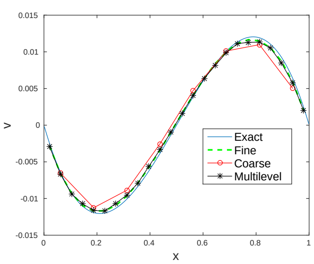

(D) v: $N = 8, y = 0.5625$

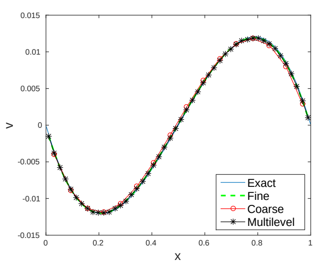

(E) v: $N = 16, y = 0.5312$

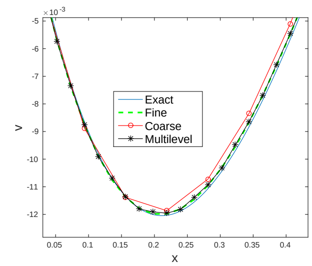

(F) Zoomed in (left 9(e))

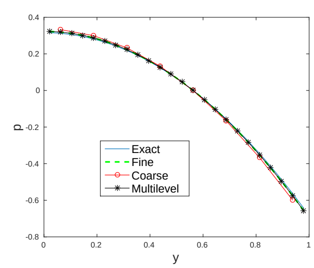

(G) $p : N = 8, x = 0.5625$

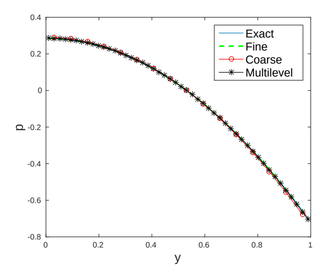

(H) $p : N = 16, x = 0.5312$

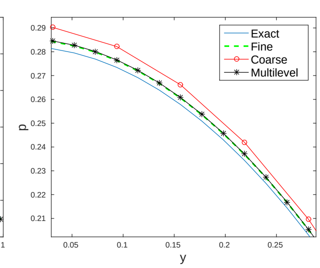

(I) Zoomed in (left 9(h))

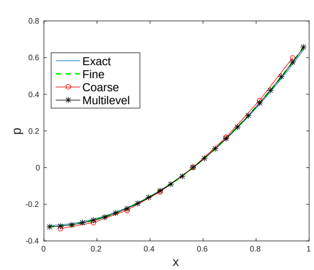

(J) $p : N = 8, y = 0.5625$

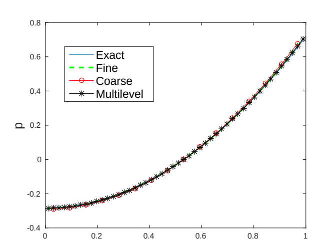

(K) $p : N = 16, y = 0.5312$

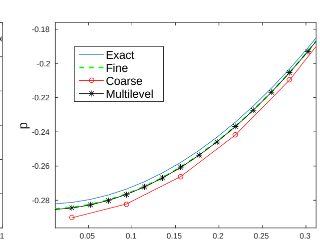

(L) Zoomed in (left 9(k))

FIGURE 9. Velocities and pressure obtained from explicit methods when $\Delta t = 10^{-4}$ for some x and y at $T = 0.001$ for Example 2.

Example 2

We consider the exact solutions [15]

$$u(x, y, t) = (t + 1)^2\, x^2\, (1 - x)^2\, (2y - 6y^2 + 4y^3)$$
$$v(x, y, t) = (t + 1)^2\, y^2\, (1 - y)^2\, (-2x + 6x^2 - 4x^3)$$
$$p(x, y) = x^2 - y^2,$$

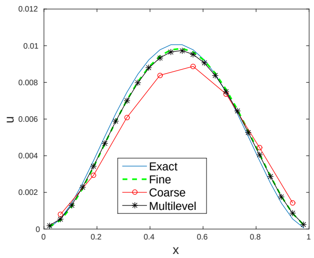

(A) $u : N = 8, y = 0.3125$

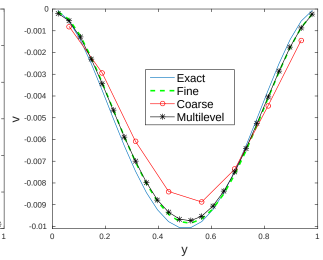

(B) $v : N = 8, x = 0.3125$

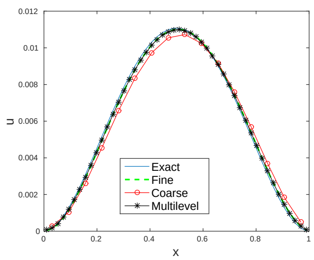

(C) $u : N = 16, y = 0.2812$

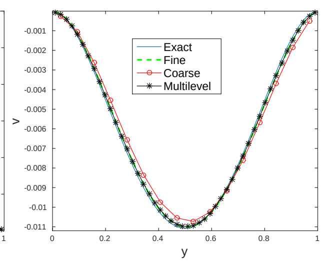

(D) $v : N = 16, x = 0.2812$

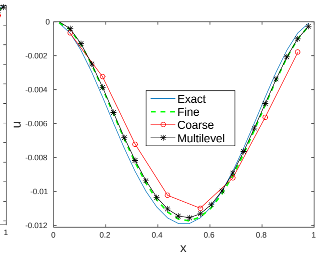

(E) $u : N = 8, y = 0.8125$

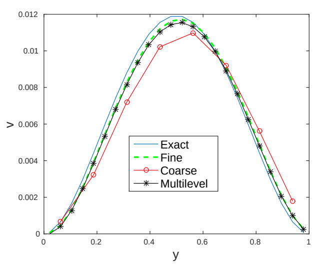

(F) $v : N = 8, x = 0.8125$

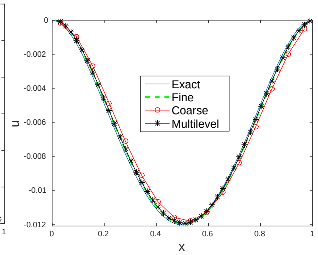

(G) $u : N = 16, y = 0.7812$

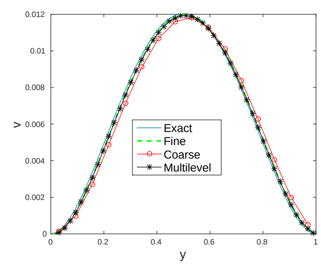

(H) $v : N = 16, x = 0.7812$

FIGURE 10. Velocities obtained from explicit methods when $\Delta t = 10^{-4}$ for some cell centres x and y at $T = 0.001$ for Example 2.

where the source term is obtained on substitution to the equation (2). The initial condition of the velocity is obtained by substituting $t = 0$. In this example we consider $T = 0.001$ and two time steps, $\Delta t = 10^{-5}$ and $\Delta t = 10^{-4}$. The L^2-errors obtained from the numerical methods with their CPU time are given in Table 2. Exact velocities and pressure are shown in Figures 4(a)-4(c). Figure 5 shows the 2D plots for the peak velocities when $\Delta t = 10^{-5}$ at some cells for $N = 16$. The 3D numerical profiles obtained from the explicit methods, when the time step is $\Delta t = 10^{-4}$, are shown in Figures 6(d)-6(l) and from the implicit methods are given by Figure 7. The absolute error fields obtained from the multilevel and the one-level method on the fine mesh are shown by Figure 8. Figures 9-12 show the 2D plots of the velocities and pressure obtained from the numerical methods for some selected cells.

From Tables 1-3, we can see that the multilevel methods are intermediate between the one-level methods on the fine mesh and on the coarse mesh.

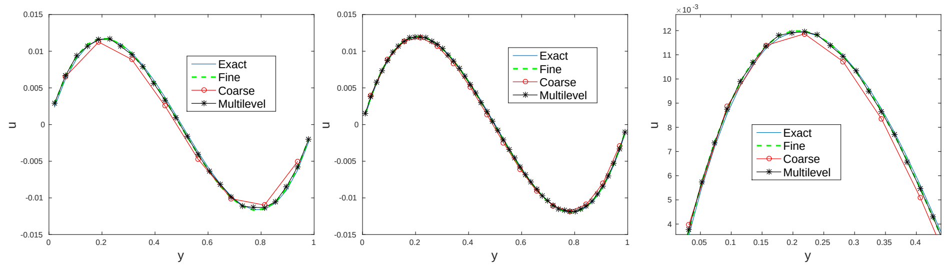

(A) u: $N = 8, x = 0.5625$ (B) u: $N = 16, x = 0.5312$ (C) Zoomen in (left 11(b))

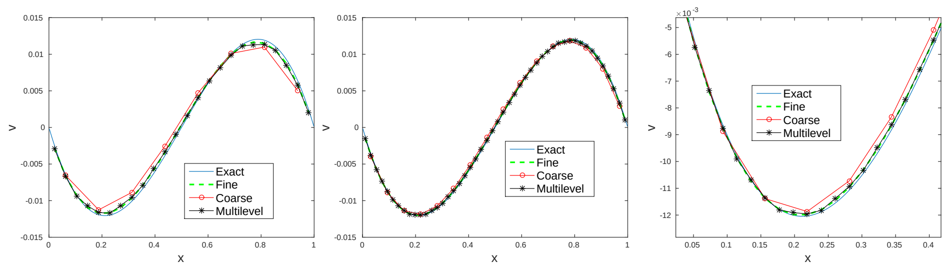

(D) v: $N = 8, y = 0.5625$ (E) v: $N = 16, y = 0.5312$ (F) Zoomed in (left 11(e))

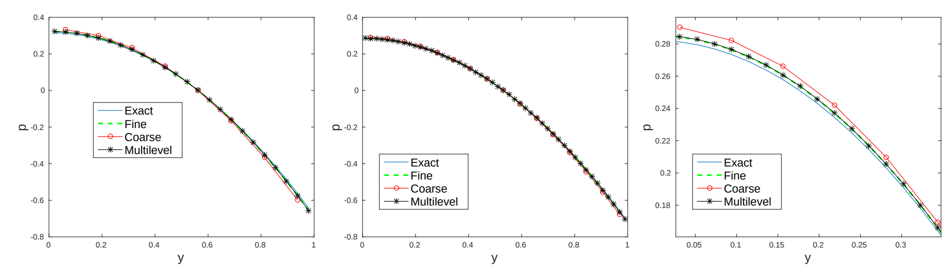

(G) $p : N = 8, x = 0.5625$ (H) $p : N = 16, x = 0.5312$ (I) Zoomed in (left 11(h))

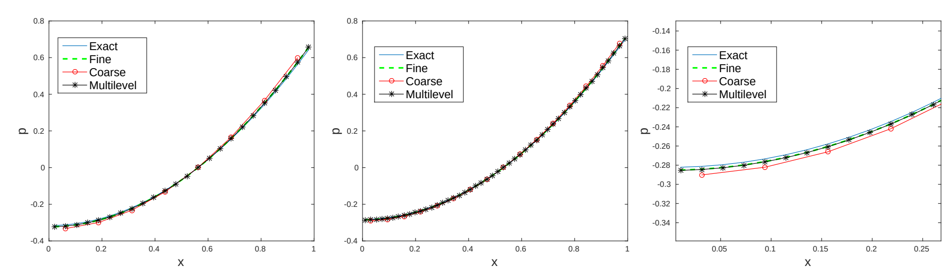

(J) $p : N = 8, y = 0.5625$ (K) $p : N = 16, y = 0.5312$ (L) Zoomed in(left 11(k))

FIGURE 11. Velocities and pressure obtained from implicit methods when $\Delta t = 10^{-4}$ for some x and y at $T = 0.001$ for Example 2.

Example 3: The driven cavity problem

The driven cavity problem is a standard benchmark for testing the performance of numerical methods for incompressible Navier-Stokes equations [16]. This problem has been studied by several researchers where the most detailed was studied by

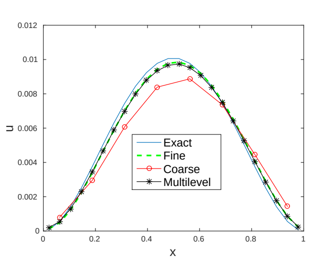

(A) $u : N = 8, y = 0.3125$

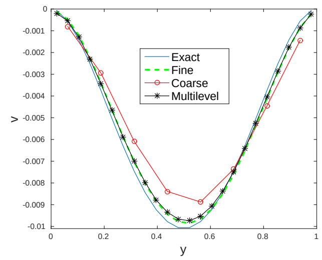

(B) $v : N = 8, x = 0.3125$

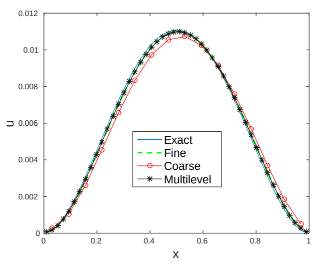

(C) $u : N = 16, y = 0.2812$

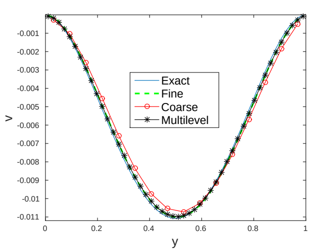

(D) $v : N = 16, x = 0.2812$

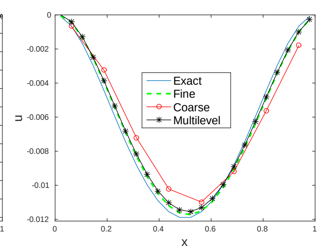

(E) $u : N = 8, y = 0.8125$

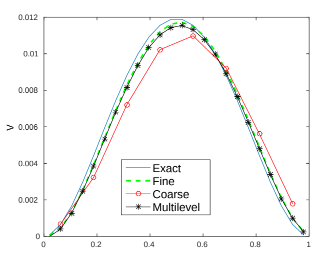

(F) $v : N = 8, x = 0.8125$

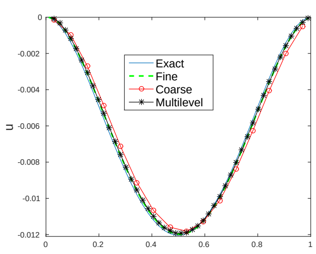

(G) $u : N = 16, y = 0.7812$

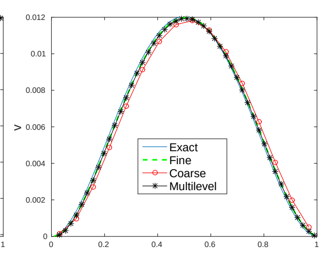

(H) $v : N = 16, x = 0.7812$

FIGURE 12. Velocities obtained from implicit methods when $\Delta t = 10^{-4}$ for some cell centres x and y at $T = 0.001$ for Example 2.

Ghia et al [17] in which they quote many solutions and data for different Reynolds numbers. We consider the square cavity problem corresponding to a flow in a unit square domain ($\Omega = [0,1] \times [0,1]$) with tangential velocity prescribed on the top boundary to a normalized value $u = 1$, which is given as follows:

$$u_{i,N+1} = 1, u_{i,0} = u_{0,j} = u_{N,j} = 0,$$
$$v_{i,N+1} = v_{i,0} = v_{0,j} = v_{N,j} = 0,$$

for $i = 1, \ldots, N$ and $j = 1, \ldots, N$. The velocity profiles are compared with the benchmark solutions by Ghia et al. [17]. Here, we present the numerical results obtained in the simulation of the driven cavity flow, until the long term time independent steady state solution is achieved. A steady state is achieved at $T = 10$, where the relative error between the two time steps reached below a value 10^{-4}. Figure 13 illustrates the u-velocity along the vertical line passing through the center $x = 1/2$ and the v-velocity along the horizeontal line passing through the center $y = 1/2$. The computations have been done for the Renolds number Re$= \frac{1}{\nu} = 100$

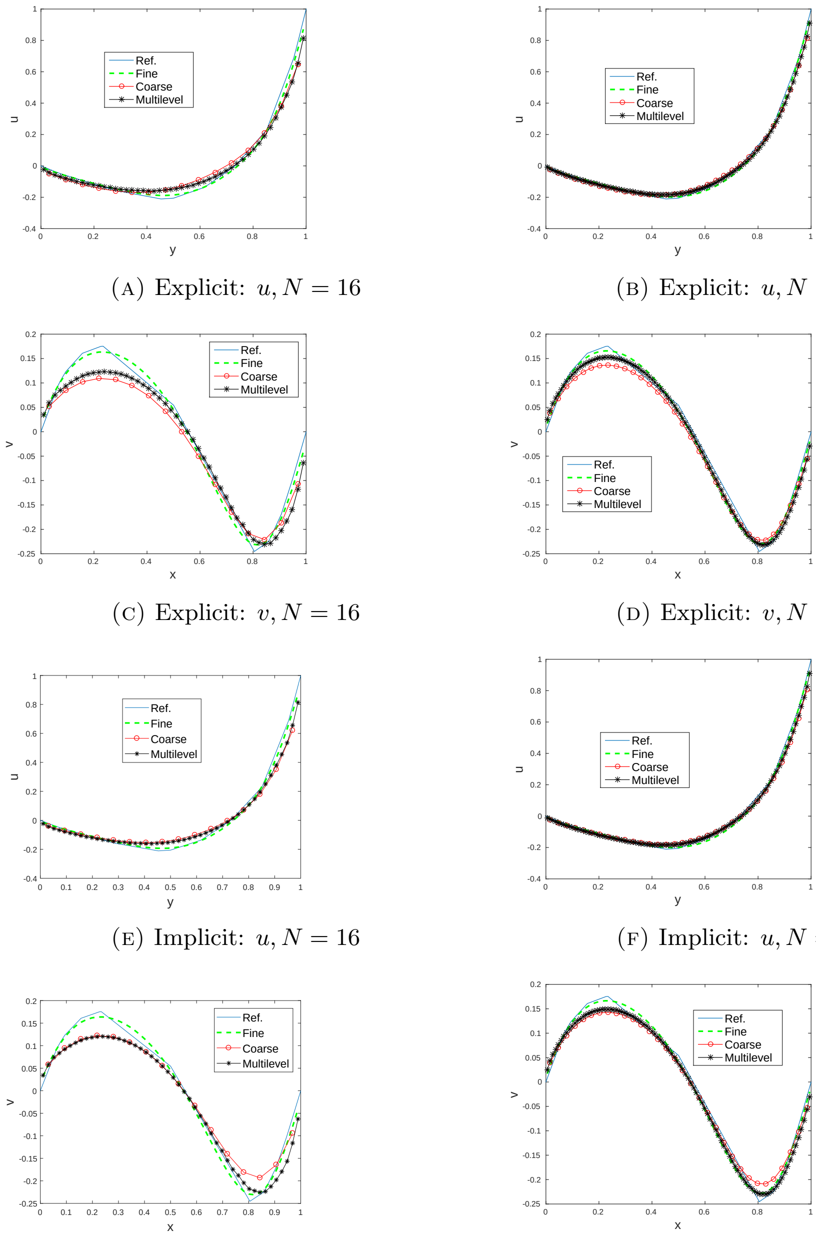

(A) Explicit: $u, N = 16$

(B) Explicit: $u, N = 32$

(C) Explicit: $v, N = 16$

(D) Explicit: $v, N = 32$

(E) Implicit: $u, N = 16$

(F) Implicit: $u, N = 32$

(G) Implicit: $v, N = 16$

(H) Implicit: $u, N = 32$

FIGURE 13. Driven cavity: profiles of velocities from implicit methods when $\Delta t = 10^{-2}$ at $T = 10$.

with $N = 16$, $N = 32$ and $\Delta t = 0.01$. The velocities at the centrelines are calculated by taking the average of the values of the neighboring cells, that is, cells with centres at $1/2 \pm \Delta x/2$ and $1/2 \pm \Delta y/2$, for the u-velocity and v-velocity, respectively.

TABLE 1. CPU time and Errors when $\Delta t = 0.0001$ at $T = 0.01$.

Methods		N	L^2_u-error	Rate	L^2_p-error	Rate	CPU time
Implicit	Fine	16	6.0064×10^{-4}		0.0135		46.966
		32	3.1144×10^{-4}	0.9475	0.0085	0.6674	363.694
		64	1.5830×10^{-4}	0.9763	0.0037	1.1999	4448.832
	ML	16	0.0020		0.0134		7.075
		32	8.6070×10^{-4}	1.3539	0.0074	0.8566	47.803
		64	3.0992×10^{-4}	1.4736	0.0057	0.3766	548.532
	Coarse	16	0.0017		0.0273		1.402
		32	8.8301×10^{-4}	0.9450	0.0171	0.6749	3.937
		64	4.5744×10^{-4}	0.9488	0.0114	0.5850	20.802
Explicit	Fine	16	6.0056×10^{-4}		0.0136		7.263
		32	3.1139×10^{-4}	0.9476	0.0086	0.6612	25.399
		64	1.5824×10^{-4}	0.9766	0.0038	1.1783	85.393
	ML	16	0.0020		0.0133		1.741
		32	8.5996×10^{-4}	1.3552	0.0075	0.8265	4.134
		64	3.0661×10^{-4}	1.4879	0.0056	0.4215	14.572
	Coarse	16	0.0017		0.0268		0.621
		32	8.8263×10^{-4}	0.9457	0.0173	0.6315	1.036
		64	4.5710×10^{-4}	0.9493	0.0113	0.6144	2.681

TABLE 2. CPU time and Errors when $\Delta t = 0.00001$ at $T = 0.001$.

Methods		N	L^2_u-error	Rate	L^2_p-error	Rate	CPU time
Implicit	Fine	16	2.3034×10^{-4}		0.0043		85.053
		32	1.1690×10^{-4}	0.9785	0.0022	0.9668	422.695
		64	5.9377×10^{-5}	0.9773	0.0013	0.7590	4621.472
	ML	16	5.2706×10^{-4}		0.0044		12.618
		32	1.7704×10^{-4}	1.5739	0.0025	0.8156	57.843
		64	6.8815×10^{-5}	1.3633	0.0019	0.3959	582.124
	Coarse	16	6.6442×10^{-4}		0.0130		2.668
		32	3.4151×10^{-4}	0.9602	0.0064	1.0224	7.744
		64	1.7391×10^{-4}	0.9819	0.0032	1.0000	28.734
Explicit	Fine	16	2.3034×10^{-4}		0.0043		45.761
		32	1.1690×10^{-4}	0.9785	0.0022	0.9668	74.554
		64	5.9376×10^{-5}	0.9773	0.0013	0.7590	271.386
	ML	16	5.2706×10^{-4}		0.0044		7.078
		32	1.7704×10^{-4}	1.5739	0.0025	0.8156	13.278
		64	6.8815×10^{-5}	1.3633	0.0019	0.3959	44.111
	Coarse	16	6.6442×10^{-4}		0.0130		1.422
		32	3.4151×10^{-4}	0.9602	0.064	1.0224	4.299
		64	1.7391×10^{-4}	0.9736	0.0032	1.0000	10.307

7. Conclusion

In this paper, two numerical methods have been presented and analyzed. The implicit multilevel method discussed here is linear and easy to implement. The two multilevel methods are conditionally stable, where the implicit scheme is unconditionally stable for large values of viscosity. We compare the multilevel methods

TABLE 3. CPU time and Errors when $\Delta t = 10^{-4}$ at $T = 0.001$.

Methods		N	L^2_u-error	Rate	L^2_p-error	Rate	CPU time
Implicit	Fine	8	4.5068×10^{-4}		0.0086		2.208
		16	2.3034×10^{-4}	0.9683	0.0043	1	8.504
		32	1.1690×10^{-4}	0.9785	0.0021	1.0339	41.009
		64	5.9389×10^{-5}	0.9770	0.0012	0.8074	450.003
	ML	8	4.8847×10^{-4}		0.0087		1.184
		16	2.3860×10^{-4}	1.0337	0.0044	0.9835	2.631
		32	1.1910×10^{-4}	1.0024	0.0024	0.8745	9.513
		64	6.0106×10^{-5}	0.9866	0.0018	0.4150	94.738
	Coarse	8	0.0013		0.0261		0.227
		16	6.6441×10^{-4}	0.9684	0.0130	1.0055	0.379
		32	3.4149×10^{-4}	0.9602	0.0064	1.0224	0.829
		64	1.7390×10^{-4}	0.9736	0.0031	1.0458	2.850
Explicit	Fine	8	4.4652×10^{-4}		0.0086		1.426
		16	2.2986×10^{-4}	0.9580	0.0043	1	4.671
		32	1.1686×10^{-4}	0.9760	0.0022	0.9668	7.323
		64	5.9380×10^{-5}	0.9767	0.0013	0.7590	26.791
	ML	8	4.8847×10^{-4}		0.0087		0.817
		16	2.3860×10^{-4}	1.0337	0.0044	0.9835	1.538
		32	1.1910×10^{-4}	1.0024	0.0025	0.8156	2.180
		64	6.0090×10^{-5}	0.9870	0.0019	0.3959	6.620
	Coarse	8	0.0012		0.0261		0.149
		16	6.5015×10^{-4}	0.8842	0.0130	1.0055	0.231
		32	3.3978×10^{-4}	0.9362	0.064	1.0224	0.528
		64	1.7371×10^{-4}	0.9679	0.0032	1.0000	1.131

with the traditional one-level methods by computing the L^2-errors and CPU time. It is seen that the multilevel methods provide an efficient approach to obtaining results of good accuracy. Our future work is to extend this work to multiphase flow models.

Acknowledgments

The work of HH Gidey and BD Reddy has been supported by the National Research Foundation, through the South African Research Chair in Computational Mechanics. J.K. Djoko is funded through the incentive fund N00 401 Project 85796.

References

[1] J. Simo, F. Armero, Unconditional stability and long-term behavior of transient algorithms for the incompressible Navier–Stokes and euler equations, Computer Methods in Applied Mechanics and Engineering 111 (1-2) (1994) 111–154.

[2] A. Appadu, J. Djoko, H. Gidey, J. Lubuma, Analysis of multilevel finite volume approximation of 2d convective Cahn–Hilliard equation, Japan Journal of Industrial and Applied Mathematics 34 (2017) 253–304.

[3] A. Bousquet, M. Marion, M. Pectu, R. Temam, Multilevel finite volume methods and boundary value conditions for geophysical flows, Computers and Fluids 74 (2013) 66–90.

[4] A. Bousquet, M. Marion, R. Temam, Finite volume multilevel approximation of the shallow water equations with a time explicit scheme, International Journal of Numerical Analysis and Modeling 11 (4) (2014) 762–786.

[5] Y. He, K. Liu, A multilevel finite element method in space-time for the Navier–Stokes problem, Numerical Methods for Partial Differential Equations: An International Journal 21 (6) (2005) 1052–1078.
[6] S. Faure, J. Laminie, R. Temam, Finite volume discretization and multilevel methods in flow problems, Journal of Scientific Computing 25 (1/2) (2005) 231–261.
[7] A. Bousquet, R. Temam, A finite volume multilevel approximation of the shallow-water equations, in: J. C. F. Pereira, A. Sequeira (Eds.), European Conference on Computational Fluid Dynamics ECCOMAS CFD 2010, Vol. V, 14-17 June 2010.
[8] K. Adamy, A. Bousquet, S. Faure, J. Lamine, R. Temam, A multilevel method for finite volume discretization of the two-dimensional nonlinear shallow-water equations, Ocean Modeling 33 (2010) 235–256.
[9] A. J. Chorin, The numerical solution of the Navier-Stokes equations for an incompressible fluid, Bulletin of the American Mathematical Society 73 (6) (1967) 928–931.
[10] R. Temam, Navier–stokes equations, theory and numerical analysis, Amsterdam: NorthHolland 1 (1977) 984.
[11] J.-L. Guermond, J. Shen, Velocity-correction projection methods for incompressible flows, SIAM Journal on Numerical Analysis 41 (1) (2003) 112–134.
[12] J. Kim, P. Moin, Application of a fractional-step method to incompressible Navier-Stokes equations, Journal of Computational Physics 59 (2) (1985) 308–323.
[13] J.-L. Guermond, P. Minev, J. Shen, An overview of projection methods for incompressible flows, Computer Methods in Applied Mechanics and Engineering 195 (44-47) (2006) 6011–6045.
[14] R. Rannacher, On chorin's projection method for the incompressible Navier-Stokes equations, in: The Navier-Stokes equations IItheory and numerical methods, Springer, 1992, pp. 167–183.
[15] W. Gao, Y.-L. Duan, R.-X. Liu, The finite volume projection method with hybrid unstructured triangular collocated grids for incompressible flows, Journal of Hydrodynamics 21 (2) (2009) 201–211.
[16] O. Zienkiewicz, R. Taylor, P. Nithiarasu, The Finite Element Method for Fluid Dynamics, 7th Edition, Butterworth-Heinemann, 2014.
[17] U. Ghia, K. N. Ghia, C. Shin, High-Re solutions for incompressible flow using the Navier-Stokes equations and a multigrid method, Journal of Computational Physics 48 (3) (1982) 387–411.

African Peer Review Mechanism, Johannesburg, South Africa

Centre for Research in Computational and Applied Mechanics, University of Cape Town, 7701 Rondebosch, South Africa; Department of Mathematics and Applied Mathematics, University of Cape Town, 7701 Rondebosch, South Africa; Department of Mathematics, Aksum University, Axum, Ethiopia
E-mail: hagos.gidey@uct.ac.za

Centre for Research in Computational and Applied Mechanics, University of Cape Town, 7701 Rondebosch, South Africa; Department of Mathematics and Applied Mathematics, University of Cape Town, 7701 Rondebosch, South Africa